ARTICLES
https://doi.org/10.1038/s41556-020-00607-4

nature cell biology

Female human primordial germ cells display X-chromosome dosage compensation despite the absence of X-inactivation

Tsotne Chitiashvili[1,2,3], Iris Dror[1], Rachel Kim[4], Fei-Man Hsu[2], Rohan Chaudhari[1,2], Erica Pandolfi[2], Di Chen[2], Simone Liebscher[5], Katja Schenke-Layland[5,6,7], Kathrin Plath[1,3,4,8] ✉ and Amander Clark[2,3,4,8] ✉

X-chromosome dosage compensation in female placental mammals is achieved by X-chromosome inactivation (XCI). Human pre-implantation embryos are an exception, in which dosage compensation occurs by X-chromosome dampening (XCD). Here, we examined whether XCD extends to human prenatal germ cells given their similarities to naive pluripotent cells. We found that female human primordial germ cells (hPGCs) display reduced X-linked gene expression before entering meiosis. Moreover, in hPGCs, both X chromosomes are active and express the long non-coding RNAs X active coating transcript (*XACT*) and X inactive specific transcript (*XIST*)—the master regulator of XCI—which are silenced after entry into meiosis. We find that *XACT* is a hPGC marker, describe XCD associated with *XIST* expression in hPGCs and suggest that XCD evolved in humans to regulate X-linked genes in pre-implantation embryos and PGCs. Furthermore, we found a unique mechanism of X-chromosome regulation in human primordial oocytes. Therefore, future studies of human germline development must consider the sexually dimorphic X-chromosome dosage compensation mechanisms in the prenatal germline.

Dosage compensation of genes on the X chromosome is an essential epigenetic event that equalizes the X-linked gene imbalance between males and females[1–8]. In mice, dosage compensation is mediated by XCI[1–7], which is established early during development, first in an imprinted form and, after a brief phase of reactivation in naive pluripotent epiblast cells, through the random form by silencing either the maternal or paternal X chromosome[1–7]. Molecularly, XCI is mediated by the long non-coding RNA (lncRNA) *XIST*, which coats the X chromosome in *cis* to establish and maintain a silencing compartment over the X-chromosome territory[1–7]. Once established, XCI is stably maintained in female somatic cells; however, in female mouse primordial germ cells (mPGCs), the inactive X chromosome (Xi) is reactivated, which coincides with global epigenetic reprogramming[9–11]. Following epigenetic reprogramming, and as mPGCs differentiate into meiotic cells in females or prospermatogonia in males, germ cells display X-chromosome dosage excess or X-chromosome dosage decompensation, respectively[12], highlighting the sexually dimorphic regulation of gene expression on the X chromosome in mouse germ cells.

Despite the conservation of *XIST* and XCI across placental mammals[13], it is now appreciated that there is no evidence for the imprinted form of XCI in human pre-implantation embryos[14–16]. Moreover, in human female pre-implantation blastocysts, *XIST* is uniquely expressed from both X chromosomes[14,15,17] and the expression of X-linked genes on both alleles is transcriptionally reduced but not silenced—a compensated state that is referred to as XCD[14]. Another striking difference in humans is the existence of *XACT*, a primate-specific lncRNA that is expressed from the active X chromosome(s) in both human pre-implantation embryos and pluripotent stem cells that can oppose the function of *XIST*[14,17,18]. The expression status of *XACT* in hPGCs is unknown.

The unique XCD state in human pre-implantation embryos has been puzzling and is speculated to resolve to XCI within 1–2 weeks[19]. It has therefore been postulated that the transient accumulation of *XIST* on both X chromosomes with XCD represents the initiating stages of the normal process of XCI[20]. This interpretation is consistent with the biallelic *XIST* expression that is observed in differentiating female mouse embryonic stem cells (ESCs) during the XCI initiation process[21], yet is inconsistent with other findings that suggest that there is a transient state with two active X chromosomes (Xa) without *XIST* expression in cells transitioning between XCD and XCI[22,23]. As mouse and human PGCs capture many of the epigenetic features of epiblast cells from the pre-implantation embryo[24–26], yet hPGCs stably persist for around two months during development, we hypothesized that female hPGCs could serve as an alternative model to evaluate the possibility that XCD is an independent and stable regulatory mechanism for X-chromosome dosage compensation in humans.

Results

Female hPGCs express *XACT* from two active X chromosomes. As the expression of the X-linked lncRNA *XACT* is associated

[1]Department of Biological Chemistry, David Geffen School of Medicine, University of California Los Angeles, Los Angeles, CA, USA. [2]Molecular Cell and Developmental Biology Department, University of California Los Angeles, Los Angeles, CA, USA. [3]Molecular Biology Institute, University of California Los Angeles, Los Angeles, CA, USA. [4]Eli and Edythe Broad Center of Regenerative Medicine and Stem Cell Research, University of California Los Angeles, Los Angeles, CA, USA. [5]Department of Women's Health, Research Institute for Women's Health, Eberhard Karls University Tübingen, Tübingen, Germany. [6]NMI Natural and Medical Sciences Institute, University Tübingen, Reutlingen, Germany. [7]Department of Medicine/Cardiology, Cardiovascular Research Laboratories, David Geffen School of Medicine, University of California Los Angeles, Los Angeles, CA, USA. [8]Jonsson Comprehensive Cancer Center, University of California Los Angeles, Los Angeles, CA, USA. ✉e-mail: kplath@mednet.ucla.edu; clarka@ucla.edu

with the unique X-chromosome state of human pre-implantation embryos[14,17], we performed RNA fluorescence in situ hybridization (FISH) analysis of *XACT* in prenatal ovaries together with immunostaining for the germ cell-specific protein deleted in azoospermia like (DAZL), which marks hPGCs[27]. We observed *XACT* transcripts in nearly all female hPGCs (DAZL$^+$ cells) at weeks 7–8 post-fertilization (p.f.), whereas somatic cells (DAZL$^-$) lacked *XACT* expression (Fig. 1a,b). We identified two *XACT* clouds in approximately 60–70% of hPGCs; each of these *XACT* clouds was probably associated with the X chromosome that the RNA was transcribed from (Fig. 1c). Starting from 10 weeks p.f., hPGCs heterogeneously differentiate into meiotic germ cells in females[28], repressing pluripotency-related genes such as *NANOG*[29]. We therefore also detected NANOG to distinguish between NANOG$^+$DAZL$^+$ hPGCs and NANOG$^-$DAZL$^+$ meiotic germ cells. We discovered that *XACT* is still expressed in the majority of NANOG$^+$DAZL$^+$ female hPGCs at week 14 p.f. (Fig. 1d,e). By contrast, the majority of NANOG$^-$DAZL$^+$ meiotic germ cells are *XACT* negative (Fig. 1d,e). Thus, *XACT* is expressed from both X chromosomes in hPGCs, and is not expressed by ovarian somatic cells.

To evaluate whether additional genes encoded on the X chromosome are biallelically expressed in hPGCs, we performed RNA FISH analysis of the X-linked genes *HUWE1* and *ATRX*, detecting their nascent transcription foci in week 8 p.f. ovaries. We found that the majority of hPGCs marked by *XACT* also biallelically expresses *HUWE1* and *ATRX* (Fig. 1f–h). By contrast, the somatic cells express these genes from a single allele due to XCI (Fig. 1f–h). These results are consistent with previous allelic analysis of X-linked gene expression from 53 sorted female germ cells[30], which revealed biallelic expression of X-linked genes (Extended Data Fig. 1a). As a consequence, we conclude that female hPGCs carry two active X chromosomes.

To confirm the active state of the X chromosome in female hPGCs, we assessed trimethylation of Lys 27 of histone H3 (H3K27me3), a chromatin mark that specifically accumulates on the Xi[31,32]. In mice, newly specified female PGCs are enriched in H3K27me3 on the Xi and progressively lose this mark as the cells undergo Xi reactivation[9,11]. Given that 23% of female hPGCs have one *XACT* cloud (Fig. 1c), we evaluated whether female hPGCs show any evidence of a nuclear H3K27me3 accumulation, indicative of an Xi[31,32]. At week 4 p.f., we identified early-stage OCT4$^+$ hPGCs entering the genital ridge epithelium before induction of DAZL expression (Extended Data Fig. 1b). We found that around 10% of OCT4$^+$DAZL$^-$ female hPGCs have an Xi-like nuclear accumulation of H3K27me3, which is reduced to less than 5% at weeks 7 and 12 p.f. once the hPGCs have settled in the ovaries (Extended Data Fig. 1b–e). The lack of an H3K27me3 Xi-like enrichment suggests that the mono-allelic expression of *XACT* observed in a portion of female hPGCs is not linked to residual XCI.

As a naive-like pluripotent expression program is common to both male and female hPGCs[33], we explored whether *XACT* also marks male hPGCs. Using published bulk RNA-seq data of sorted male and female hPGCs[24,25], we detected *XACT* expression in hPGCs but not somatic cells (Fig. 1i). We confirmed this result using RNA FISH on a fetal testis at 13 weeks p.f., detecting *XACT* in 80% of NANOG$^+$ hPGCs (Fig. 1j,k). Thus, as is the case for human pre-implantation embryos, both female and male hPGCs express *XACT*.

***XACT* is expressed in male and female hPGCLCs in vitro.** The expression of *XACT* in male and female hPGCs in vivo suggested that *XACT* may be expressed from the moment of hPGC specification. Given that hPGCs are thought to be specified between weeks 2–3 p.f.[34], it is not possible to study hPGC specification in vivo. We therefore modelled hPGC specification using the differentiation of hPGC-like cells (hPGCLCs)[35] from male (UCLA2 ESC[36]) and female (MZT04-J iPSC[37]) pluripotent stem cells (PSCs), by analysing *XACT* distribution in ITGA6$^+$EPCAM$^+$ hPGCLCs and somatic cells at day 4 of differentiation (Fig. 2a). We discovered that most male hPGCLCs had one *XACT* cloud, whereas most female hPGCLCs had two (Fig. 2b–g). By contrast, >90% of the somatic cells were *XACT* negative (Fig. 2b–g). The detection of biallelic *XACT* in female hPGCLCs is consistent with maintenance of the eroded Xi in differentiating hESCs[23]. Collectively, these data uncover that the lncRNA *XACT* is a new marker of male and female hPGCs in vivo and in vitro.

***XACT* expression is epiblast specific in human embryo attachment cultures.** Given that *XACT* is expressed in NANOG$^+$ hPGCs and hPGCLCs, we next investigated *XACT* distribution during the peri-implantation window of human development using human embryo attachment culture[38,39]. Specifically, we explored the pattern of *XACT* expression in NANOG$^+$ epiblast cells versus NANOG$^-$ trophectoderm (TE) and primitive endoderm (PE) cells. We also detected the lncRNA *XIST* to uncover changes in its distribution. First, we performed RNA FISH for *XACT* and *XIST* in combination with immunostaining for NANOG in female and male human blastocysts (day 6 p.f.). At day 6 p.f., both *XIST* and *XACT* clouds could be identified on all X chromosomes (one in males and two in females) in 75% of female and 55% of male NANOG$^+$ epiblast cells (Fig. 3a,b,d,e). Furthermore, 30% of male epiblast cells also express only *XACT* (Fig. 3e). By contrast, NANOG$^-$ TE and PE cells have more diverse *XIST* and *XACT* expression states—*XACT* is more often repressed (Fig. 3c,f). These observations indicate that *XACT* expression is more strongly associated with the NANOG$^+$ epiblast. Using human embryo attachment culture[38,39] grown to day 12 p.f.—that is, the legal limit for human embryo culture in California—we discovered that the majority of female NANOG$^+$ epiblast cells continued to display *XIST* and *XACT* clouds on both X chromosomes (Fig. 3g,h), whereas male epiblast cells maintained expression of *XACT* but not *XIST* (Fig. 3j,k). In the majority of female NANOG$^-$ cells, *XACT* was repressed and *XIST* was expressed from one X chromosome (Fig. 3i), suggesting that these cells have transitioned to the initiation of XCI. By contrast, in male embryos, both lncRNAs were silenced in 70% of NANOG$^-$ cells (Fig. 3l). Together, these data reveal that *XACT* is expressed by the majority of NANOG$^+$ epiblast cells in the pre-implantation and early peri-implantation stages of male and female human embryo development. By contrast, *XIST* is rapidly repressed in male NANOG$^+$ epiblast between days 6 and 12, highlighting differences in *XIST* regulation in male and female human peri-implantation development.

Female hPGCs dampen expression from the active X chromosomes. As female hPGCs express *XACT* from both X chromosomes, our next goal was to determine whether XCD occurs in hPGCs. We performed single-cell RNA sequencing (scRNA-seq) on single-cell suspensions of five prenatal ovaries and five prenatal testes from weeks 6 to 16 p.f. (Fig. 4a–c). This unbiased approach yielded a total of ~50,000 prenatal gonadal cells, including ~281 male and 1,938 female germ cells that were used to analyse the ratio of X-linked gene expression to autosome gene expression (X/A ratio; a summary of which is provided in Supplementary Table 1).

Calculating the X/A ratio across individual cells per developmental age revealed that female germ cells consistently had a higher X/A ratio compared with male germ cells (Extended Data Fig. 2a,b). This difference between female and male germ cells arises from the significantly lower X-linked gene expression in males (Extended Data Fig. 2c). By contrast, we found no difference in the X/A ratio between male and female gonadal somatic cells (Extended Data Fig. 2a,b). We confirmed these results using a published scRNA-seq dataset of c-KIT and size-selected germ cells[40], in which germline cells are called fetal germ cells (FGCs) (Extended Data Fig. 2d,e).

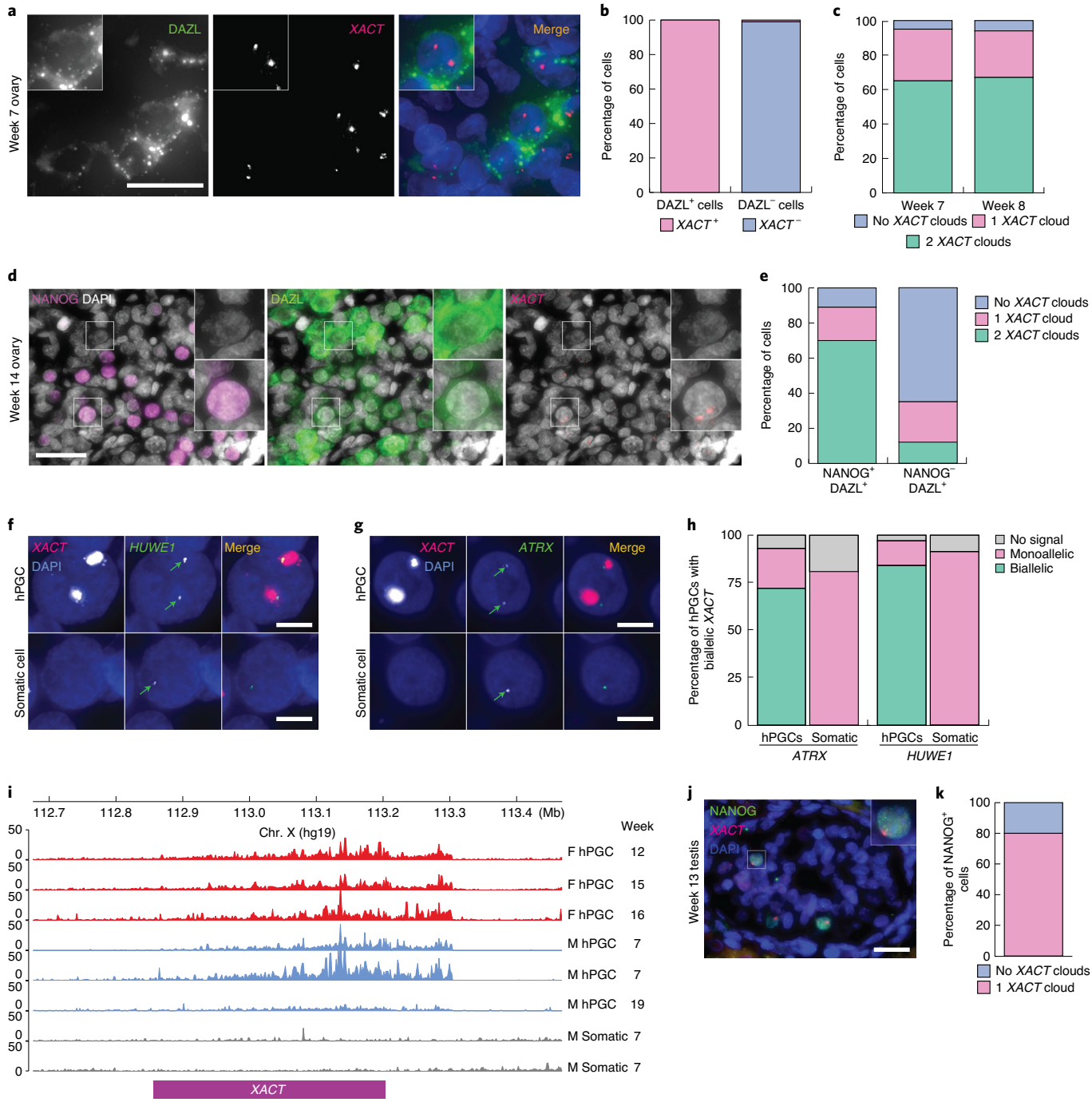

Fig. 1 | Male and female hPGCs express the lncRNA *XACT* and female hPGCs carry two active X chromosomes in vivo. a, Immuno-RNA FISH analysis of DAZL (green) and *XACT* (red) in a week 7 p.f. prenatal ovary with DAPI staining (blue) to detect nuclei. Scale bar, 30 µm. Inset zoom 1.2×. $n=1$ pair of ovaries. **b**, Quantification of cells with *XACT* clouds on the basis of the experiment shown in **a**. $n=100$ cells. **c**, Quantification of the number of *XACT* clouds in DAZL⁺ hPGCs at weeks 7 and 8 p.f. $n=100$ cells per time point. **d**, Immuno-RNA FISH analysis of, NANOG (magenta), DAZL (green), *XACT* (red) and DAPI (grey) in a week 14 p.f. fetal ovary. $n=1$ pair of ovaries. Insets: a NANOG⁻DAZL⁺ hPGC negative for *XACT* (top); and a NANOG⁺DAZL⁺ hPGC with two *XACT* clouds (bottom). Scale bar, 30 µm. Inset zoom 2.5×. **e**, Quantification of the proportion of cells with different *XACT* cloud patterns in the hPGCs (NANOG⁺DAZL⁺) and differentiating hPGCs (NANOG⁻DAZL⁺) from **d**. $n=92$ and $n=95$ cells, respectively, were assessed. **f**,**g**, Representative RNA FISH images for detecting nascent transcripts of the X-linked genes *HUWE1* (**f**) and *ATRX* (**g**), which are both normally subject to XCI, in a week 8 p.f. ovary. hPGCs are marked by *XACT* expression. The experiments were performed twice with similar results. Scale bar, 15 µm. **h**, Signal quantification for **g**. $n=60$ and $n=70$ cells for *ATRX* and *HUWE1*, respectively. **i**, Published bulk RNA-seq reads mapped to the *XACT* genomic locus in female (F) hPGCs (red, isolated using c-KIT^{bright} or using INTa6/EpCAM), male (M) hPGCs (blue, enriched for TNAP/KIT expression) and gonadal somatic cells (grey)[25,52,53]. Chr., chromosome. **j**, Immuno-RNA FISH of *XACT* (red), NANOG (green) and DAPI (blue) in fetal male testes at week 13 p.f. $n=1$ pair of testes. Scale bar, 30 µm. Inset zoom 2.5×. **k**, Quantification of the proportion of cells with one *XACT* cloud in NANOG⁺ male hPGCs from **j**. $n=75$ cells. Source data are available online.

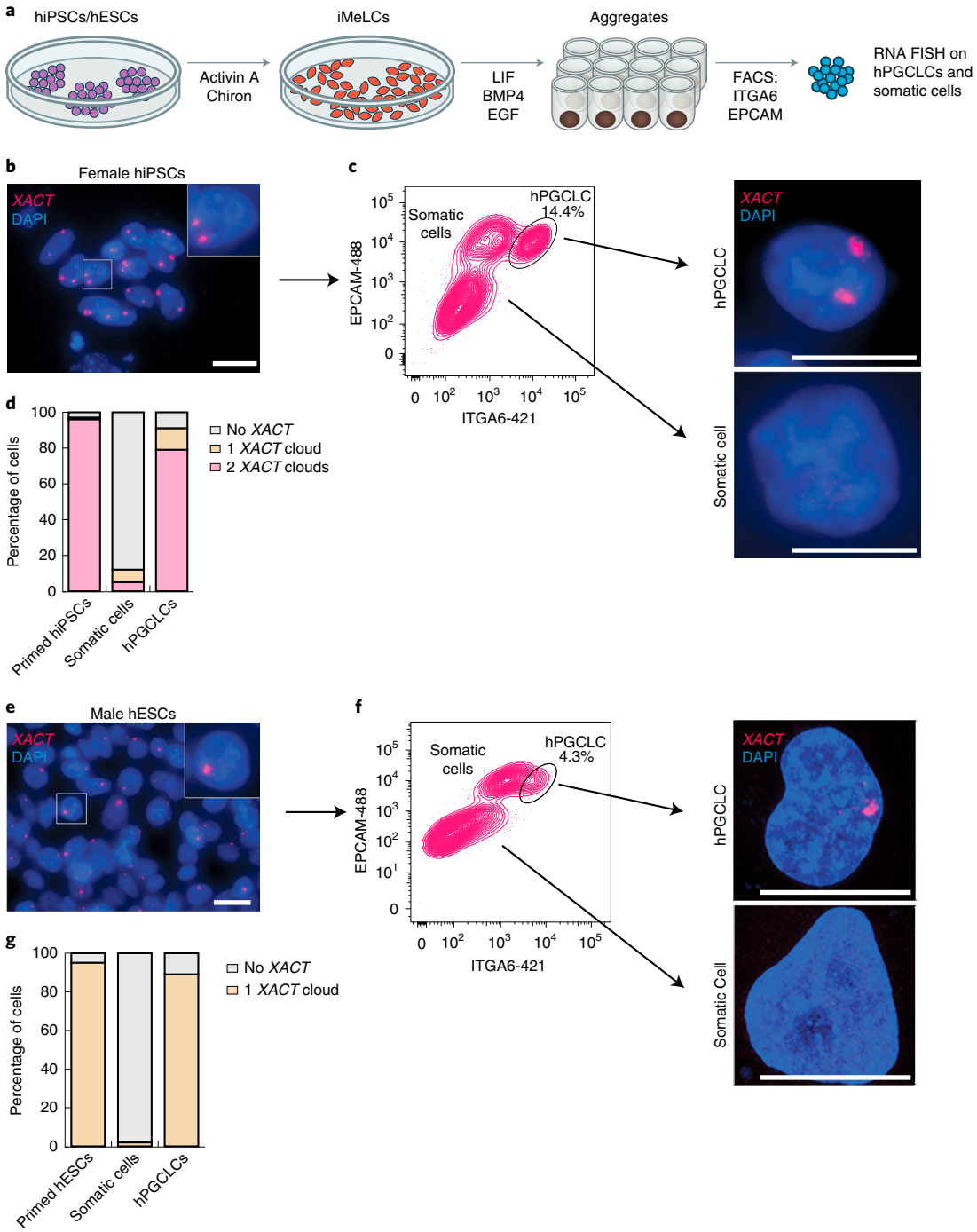

Fig. 2 | The lncRNA *XACT* is restricted to male and female hPGCLCs and is not expressed in somatic cells in vitro. a, Differentiation of hPGCLCs from human induced PSCs (hiPSCs) or hESCs through an incipient mesoderm-like cell (iMeLC) intermediate. PGCLCs and somatic cells within the aggregates were separated at day 4 by fluorescence-activated cell sorting (FACS) using antibodies against EPCAM and ITGA6. **b**, RNA FISH analysis of *XACT* in primed female hiPSCs (MZT04-J) that harbour an Xa and an eroded X chromosome with *XACT* (red) and DAPI (blue) staining. *XACT* clouds were detected from the Xa and eroded X chromosome. Scale bar, 20 μm. Inset zoom 2.5×. The experiments were performed twice with similar results. **c**, Female hiPSCs were differentiated to hPGCLCs and isolated from the aggregates using FACS at day 4 (left). The hPGCLC population is indicated. Right, *XACT* RNA FISH analysis of hPGCLCs and somatic cells. The experiments were performed twice with similar results. Scale bar, 10 μm. **d**, Quantification of the proportion of cells with different numbers of *XACT* clouds in starting hiPSCs ($n=100$ cells), hPGCLCs ($n=82$ cells) and somatic cells ($n=100$ cells) from **c**. **e**, RNA FISH analysis of *XACT* (red) in male hESCs (UCLA2). Scale bar, 20 μm, inset zoom 2.5×, similar to **b**. **f**, FACS (left) and *XACT* RNA FISH (right) analyses as described in **c**, except for with UCLA2 hESCs; the experiments were performed twice with similar results. Scale bar, 10 μm. **g**, Quantification of the proportion of cells with a different number of *XACT* clouds in UCLA2 hESCs ($n=100$ cells) and derived hPGCLCs ($n=92$ cells) and somatic cells ($n=100$ cells pooled from the two experiments). Source data are available online.

Thus, the X/A ratio is higher in female germ cells relative to male germ cells, whereas male and female gonadal somatic cells are equivalent.

As germ cell differentiation into meiotic cells is heterogeneous, we created an unsupervised developmental trajectory[41], which ordered female human germ cells across 11 clusters (Fig. 4d,e). Clusters 0–5 represent hPGCs expressing the transcription factors *NANOG* and *OCT4*, together with the hPGC markers *NANOS3*, *PRDM1* and *SOX17* (Fig. 4d). Starting in cluster 6, we observed downregulation of naive-like pluripotency genes and upregulation of the meiotic licensing gene *STRA8* (ref. [42]) and of genes encoding RNA-binding proteins such as *DAZL* and *DDX4* (also known as *VASA*; clusters 6–7). This was followed by expression of the meiotic prophase I genes *SPO11* and *SYCP1* in clusters 8–9 and, ultimately, in cluster 10, upregulation of primordial oocyte genes including the zona pellucida protein 3 (*ZP3*)[43] (Fig. 4d). Thus, consistent with previous reports[24–26,28,30,40], our data capture the heterogenous differentiation of female hPGCs into meiotic germ cells beginning around week 9–10 p.f., which results in a complex mixture of germ cells including hPGCs, meiotic germ cells and primordial oocytes in a given prenatal ovary (Fig. 4f).

Analysis of the X/A ratio in female germ cells along the developmental trajectory (Fig. 5a) showed that, as hPGCs begin differentiating into meiotic germ cells (cluster 6 onwards), the X/A ratio increases, reaching maximal levels in cluster 9 before precipitously dropping in primordial oocytes (cluster 10). Moreover, the X/A ratio in hPGCs (clusters 0–5) is lower than in gonadal somatic cells (Fig. 5a and Extended Data Fig. 3a–c). The median X/A ratio in hPGCs (clusters 0–5) is significantly lower compared with meiotic germ cells (clusters 6–9) but higher compared with primordial oocytes (cluster 10; Fig. 5b). These changes were largely due to changes in X-linked gene expression (Extended Data Fig. 3d,e). We confirmed these observations in the FGC scRNA-seq data[40]. Similar to our analysis, female FGCs displayed a slightly lower X/A ratio compared with the X/A ratio in gonadal somatic cells in the hPGC state, as well as a subtle, albeit significant, increase in the X/A ratio after expression of *STRA8* (Extended Data Fig. 3f,g). On the basis of these results, we conclude that the dosage of X-linked genes is dampened in female hPGCs and that this dosage compensation is erased as cells enter prophase I of meiosis I.

To evaluate X/A ratios in male prenatal germ cells, we ordered the cells along a developmental trajectory, which divided the male germ cells from week 6–16 p.f. gonads into five clusters (0–4)—the hPGC program corresponded to clusters 0–3 and cluster 4 captured differentiating germ cells (prospermatogonia; Extended Data Fig. 4a,b). In contrast to female germ cells that exhibit X-chromosome dosage excess with exit from the hPGC state, the X/A ratio does not change when male hPGCs differentiate into prospermatogonia (Extended Data Fig. 4c–h), which was confirmed with published datasets[40] (Extended Data Fig. 4i,j). Thus, an increase in X/A ratio as hPGCs differentiate is a female-specific phenomenon that is associated with entrance into prophase I of meiosis I.

XCD in female hPGCs is associated with *XIST* expression. To evaluate whether XCD in female hPGCs is associated with the expression of *XIST*, as has been shown in female human pre-implantation embryos, we examined *XIST* in individual female germ cells along the developmental trajectory. We discovered that *XIST* expression is significantly higher in hPGCs (clusters 0–5) compared with meiotic germ cells (clusters 6–9) and primordial oocytes (cluster 10; Fig. 5c,d). This result was also validated in the female FGC dataset[40] (Extended Data Fig. 5a). In agreement with the low expression of *XIST* in primordial oocytes, the levels of the RNA are also low in adult oocytes[44] (Extended Data Fig. 5b). Thus, the increase in the X/A ratio from hPGCs to meiotic germ cells is accompanied by a decrease in *XIST* transcript levels (Fig. 5b,d and Extended Data Fig. 5c). Consistent with this result, when analysing hPGCs and meiotic germ cells together (clusters 0–9) on the basis of *XIST* expression, *XIST*$^+$ cells displayed a significantly lower X/A ratio compared with *XIST*$^-$ cells. Primordial oocytes (cluster 10) have an even lower X/A ratio, yet express *XIST* at the lowest level (Fig. 6b,d and Extended Data Fig. 5d).

Next, we evaluated the localization of *XIST* in female hPGCs using RNA FISH from week 7 to week 14 p.f., using *XACT* as a marker of hPGCs. We found that *XIST* is detectable in the vast majority of *XACT*-expressing hPGCs, with diverse patterns of the *XIST* signal (Fig. 6a–c). These include (1) an eroded cloud pattern, whereby *XIST* is restricted over one X chromosome in a pattern that is characteristic of Xi localization, yet less enriched compared with the Xi in somatic cells, combined with a nascent transcription spot of *XIST* on the second X chromosome; (2) a dispersed configuration whereby the *XIST* signal is detected throughout a large portion of the nucleus albeit in the vicinity of both *XACT* clouds, suggesting that *XIST* is expressed from both X chromosomes; (3) one dot in the vicinity of one of the two *XACT* signals, indicating expression from one X chromosome; and (4) two dots representing the nascent transcription sites of *XIST* on both X chromosomes (Fig. 6a). Quantification of the *XIST* expression patterns in female hPGCs with two *XACT* clouds—which enabled the localization of both X chromosomes—revealed that the majority of hPGCs (58%) at week 7 p.f. had a dispersed *XIST* signal (Fig. 6c). Around 6% of cells with biallelic *XACT* expression displayed an eroded *XIST* cloud pattern and 19% and 15%, respectively, exhibited mono- and biallelic nascent *XIST* transcription foci (Fig. 6c). At later stages of embryo development (week 8 and week 14 p.f.), *XACT*$^+$ female hPGCs displayed similar patterns of *XIST* RNA with an increasing fraction of *XIST*$^-$ cells (Fig. 6b,c).

As we observed an Xi-like distribution of *XIST* in 6% of week 7 and 8 p.f. hPGCs with two *XACT* clouds, we tested whether female

Fig. 3 | *XACT* is predominantly expressed in NANOG$^+$ pre- and post-implantation epiblast cells. a,**d**,**g**,**j**, Immuno-RNA FISH analysis of NANOG (white), *XIST* (green) and *XACT* (red) in day 6 p.f. intact female pre-implantation blastocysts (**a**) ($n=2$ blastocysts); day 6 p.f. male pre-implantation blastocysts (**d**) ($n=3$ blastocysts); female embryos cultured to day 12 p.f. using human embryo attachment culture (**g**) ($n=3$ embryos); and male human embryos cultured to day 12 p.f. using human embryo attachment culture (**j**) ($n=2$ embryos). Scale bars, 30 µm. For **a**, **d**, **g** and **j**, insets: NANOG$^+$ (blue) nuclei with *XIST* and *XACT* clouds. Inset zoom 7.5×. **b**, Quantification of the proportion of cells with different numbers of *XIST* and *XACT* clouds in NANOG$^+$ epiblast cells from the female blastocysts shown in **a**; 17 cells were analysed in 2 blastocysts. **c**, Quantification of the RNA pattern in NANOG$^-$ TE and PE cells from the female blastocysts shown in **a**. $n=111$ cells quantified from the 2 blastocysts. **e**, Quantification of the proportion of cells with different numbers of *XIST* and *XACT* clouds as described in **b** from the NANOG$^+$ epiblast cells from the male blastocysts shown in **d**. $n=24$ cells from 3 blastocysts counted. **f**, Quantification of the RNA pattern as described in **c**, except for with NANOG$^-$ TE and PE cells from the male blastocysts shown in **d**; $n=180$ cells from 3 blastocysts were counted. **h**, Quantification of the proportion of cells with different numbers of *XIST* and *XACT* clouds as described in **b** for the female day 12 embryos from **g**; $n=67$ cells from 3 embryos were counted. **i**, Quantification of the RNA pattern as described in **c** for the female day 12 embryos shown in **g**. $n=180$ cells from 3 embryos counted. **k**, Quantification of the proportion of cells with different numbers of *XIST* and *XACT* clouds as described in **b** for the male day 12 embryos from **j**. $n=70$ cells from 2 embryos were assessed. **l**, Quantification of the RNA pattern as described in **c** for the male day 12 embryos in **j**. $n=120$ cells from 2 embryos were quantified. Source data are available online.

hPGCs with one *XACT* cloud represent cells that have undergone XCI. In this case, *XACT* should be expressed from the Xa and *XIST* from the Xi. However, we found that *XIST* is typically expressed from the same X chromosome as *XACT* in cells with monoallelic *XIST*/*XACT* expression (Fig. 6d), providing additional evidence for XCD instead of XCI in female hPGCs.

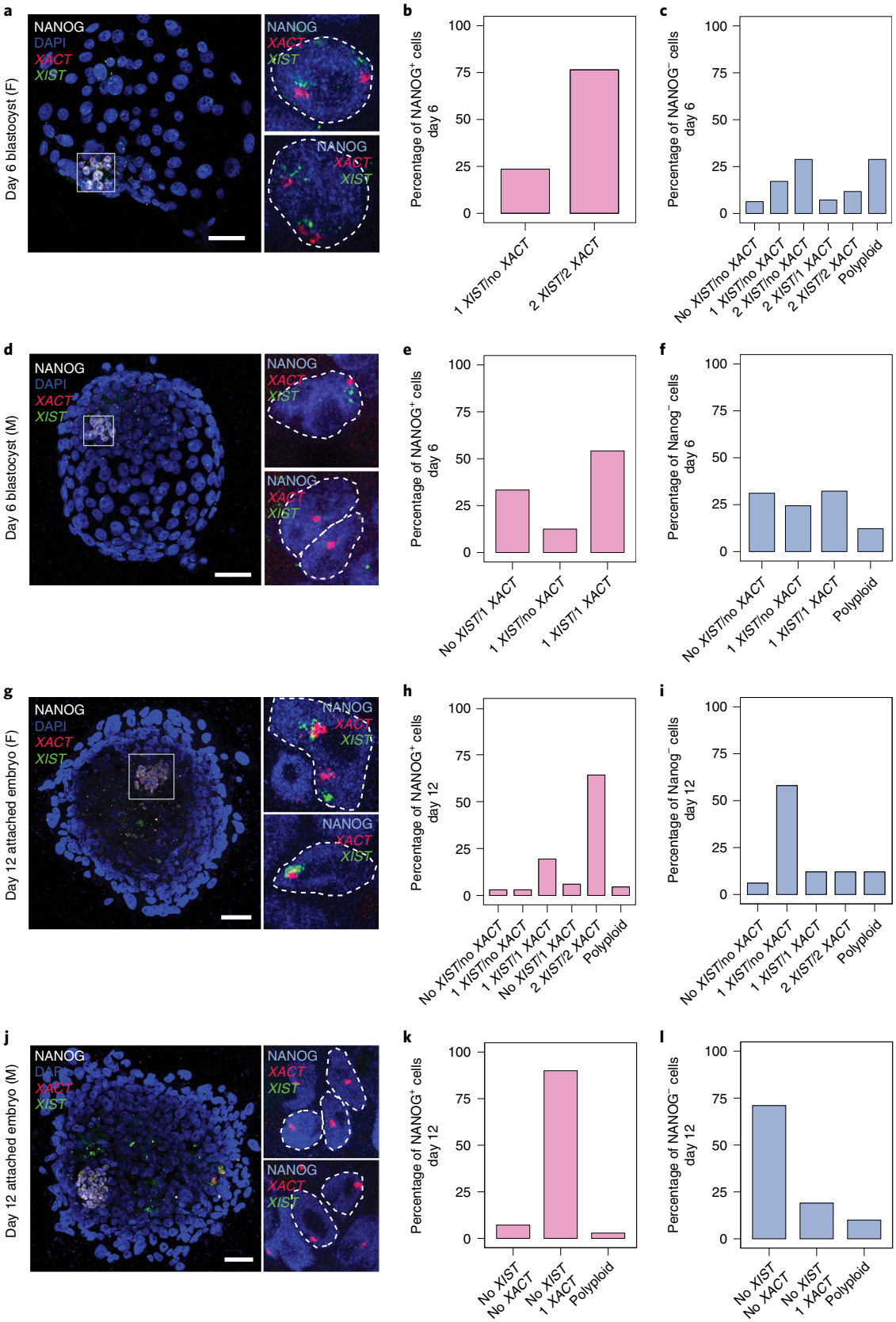

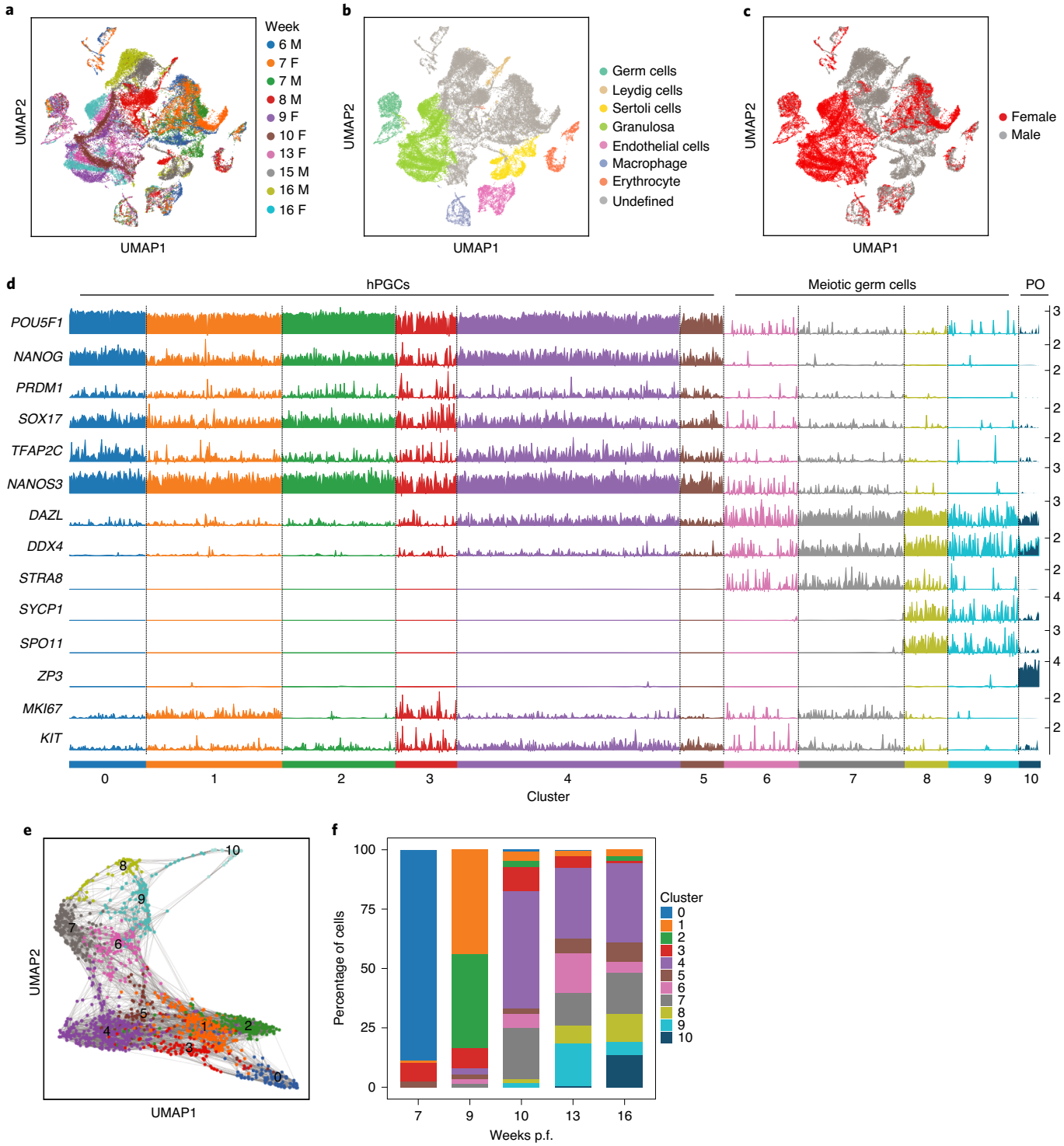

Fig. 4 | Female germ cells undergo dynamic and ordered transcriptional changes between 7-16 weeks p.f. a, The distribution of single-cell data derived from scRNA-seq from five prenatal male and five prenatal female gonads from 6–16 weeks p.f., displayed on a UMAP plot. $n = 49{,}674$ cells. **b**, Annotation of the gonadal cell types in the map in **a** on the basis of the expression of cell-type-specific markers. **c**, The distribution of male and female cells on the map from **a**. **d**, Ordering of female germ cells along the developmental trajectory from cluster 0 to cluster 10, with classification into hPGCs (clusters 0–5), meiotic germ cells (clusters 6–9) and primordial oocytes (PO, cluster 10) on the basis of diagnostic germ cell marker gene expression. Each cluster contains many individual cells (columns), for which expression of the indicated marker is given (rows). $n = 1{,}938$ cells from $n = 5$ samples. **e**, Female germ cells displayed on a UMAP plot, labelled by their cluster assignment from **d**. **f**, For each of the five female gonads described in **a**, the proportion of cells in the clusters defined in **d** is given. These data show that the repression of the pluripotency expression program and meiotic licensing (expression of *STRA8*) begins between weeks 9 and 10 p.f., and that all germ cells at week 7 are in the hPGC state. Source data are available online.

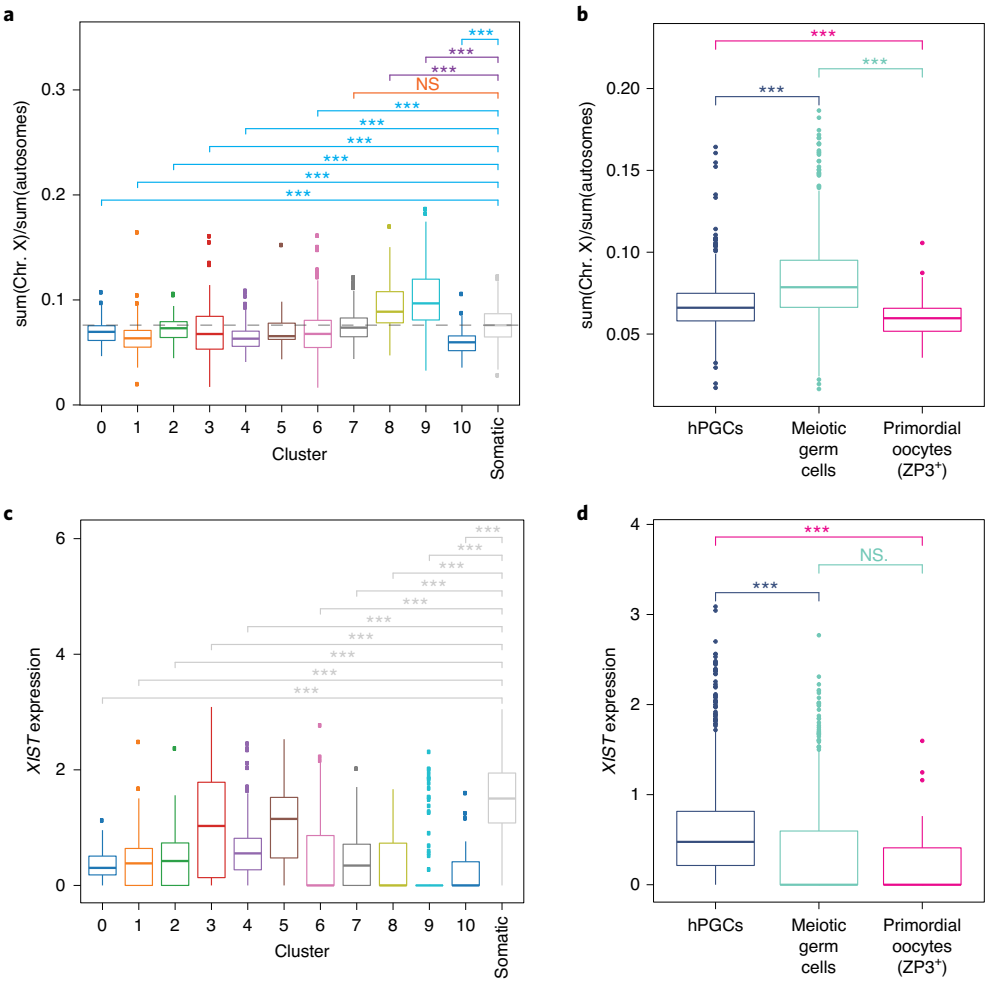

Fig. 5 | *XIST* expression is associated with XCD in female hPGCs. a, The X/A ratios in single female germ cells. $n = 1{,}938$ cells for each cluster along the developmental trajectory described in Fig. 4d. Furthermore, the X/A ratio of gonadal somatic cells are given. The dotted line indicates the median level of the X/A ratio in female somatic gonadal cells. Significance testing shows the clusters in which the X/A ratio is significantly lower compared with that in the somatic cell cluster (blue lines); the orange line shows that the difference was not significant; and the purple lines show comparisons in which the X/A ratio was significantly higher than in in the somatic cell cluster. **b**, The X/A ratios of individual female germ cells in the hPGC state, meiotic germ cell state and ZP3$^+$ primordial oocytes, merged on the basis of developmental classification (hPGC state, clusters 0–5; meiotic germ cells, clusters 6–9; and ZP3$^+$ primordial oocytes, cluster 10). **c**, Normalized counts of *XIST* transcripts in individual female germ cells for each cluster along the developmental trajectory described in Fig. 4d and female gonadal somatic cells. These results show that female hPGCs express significantly lower levels of *XIST* and there is an abrupt loss of *XIST*, which coincides with the loss of the pluripotency program in cluster 6. **d**, Normalized *XIST* transcript counts in individual female germ cells, as defined in **b**. For **a**–**d**, statistical significance was assessed using Wilcoxon tests; ns, not significant; $^{***}P < 0.001$. $n = 1{,}938$ cells analysed across 5 independent experiments.

To confirm that the loss of *XIST* expression was associated with the differentiation of NANOG$^+$DAZL$^+$ hPGCs into NANOG$^-$DAZL$^+$ meiotic germ cells, we evaluated a fetal ovary at 14 weeks p.f. using RNA FISH. We found that *XIST* was detectable in the majority of NANOG$^+$DAZL$^+$ hPGCs, with the dispersed pattern being most prominent. By contrast, the majority of NANOG$^-$DAZL$^+$ germ cells were negative for *XIST* and the subset of cells with *XIST* expression displayed the dot-like distribution (Fig. 6e,f). The quantification suggests that cells transition from the dispersed *XIST* pattern to the two-*XIST*-dot and one-*XIST*-dot patterns before *XIST* is turned off during germ cell differentiation. Furthermore, evaluating *XIST* localization around the X chromosomes in female hPGCs relative to female human pre-implantation embryos revealed a higher degree of *XIST* dispersal in hPGCs (compare Figs. 3 and 6), suggesting that the association between *XIST* and chromatin differs between the two cell types.

In addition to detecting *XIST* expression in female hPGCs, *XIST* transcripts could also be detected in male hPGCs on the basis of scRNA-seq data, albeit at much lower level than in female cells (Extended Data Fig. 5e,f). Furthermore, a small but significant reduction in the X/A ratio in male hPGCs was correlated with a significant increase in *XIST* levels (Extended Data Figs. 4j and 5f). Thus, a subset of male hPGCs can express *XIST* and display slight dampening of X-chromosome dosage. Moreover, female germ cells that lacked *XIST* displayed an increase, albeit not significant, in the *XACT* cloud size compared with cells with *XIST* expression (Extended Data Fig. 5g). Taken together, these data suggest that *XIST* may mediate dampening of X-linked gene expression in hPGCs.

Discussion

Here, by analysing human pre-implantation embryos, human embryo attachment culture, hPGCLC differentiation in vitro and

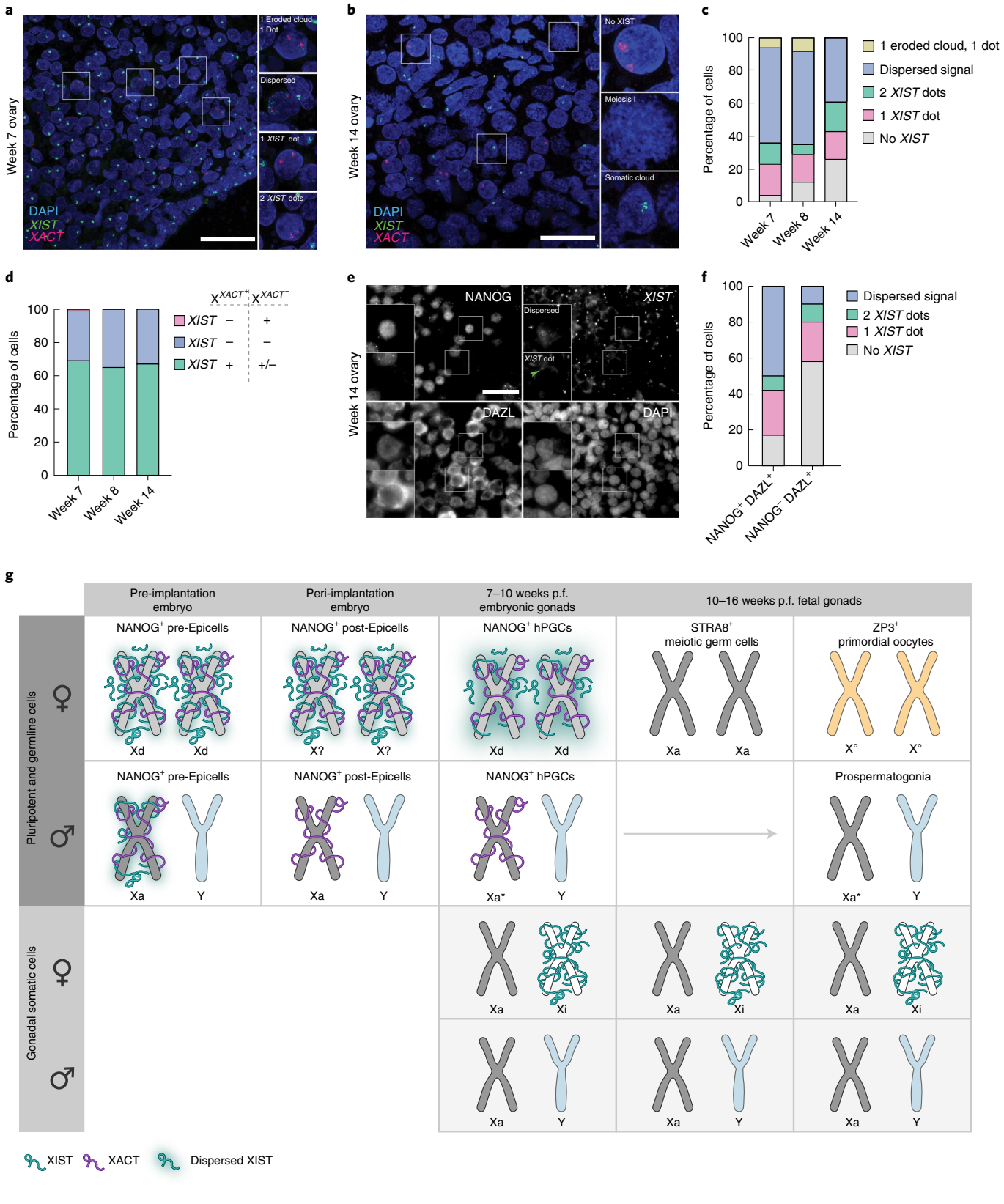

hPGCs in vivo, we revealed that the lncRNA *XACT* is expressed in pluripotent epiblast cells and hPGCs/hPGCLCs (Fig. 6g and Extended Data Fig. 6). Mechanistically, this result may be explained by the presence of an enhancer that threads *XACT* into the pluripotency network common to these cell types[45]. From this analysis, we describe that *XACT* is a unique marker of hPGCs, and speculate that it could be used to trace hPGCs from the time of lineage specification using RNA FISH. Moreover, our RNA FISH analysis of the X-linked genes *XACT*, *ATRX* and *HUWE1*, together with absence of H3K27me3 accumulation in the nucleus of most female hPGCs demonstrates that female hPGCs harbour two Xa chromosomes from at least week 4 p.f. onwards.

Fig. 6 | *XIST* is repressed as hPGCs enter meiosis. a, RNA FISH analysis of *XIST* (green) and *XACT* (red) with DAPI (blue) identifying nuclei. $n=1$ pair of ovaries (week 7 p.f.). Scale bar, 30 μm. Inset zoom 2.1×. **b**, RNA FISH as described in **a**, except for week 14 p.f. ovaries. $n=1$ pair of ovaries, scale bar, 30 μm. Inset zoom 2.6×. **c**, The proportion of cells with the indicated *XIST* expression patterns in female hPGCs with two *XACT* clouds. For each time point, $n=100$ cells from 1 pair of ovaries. **d**, The proportion of cells with the indicated *XIST* expression patterns, similar to as described in **c** except in female hPGCs with a single *XACT* cloud. Cells with a dispersed *XIST* signal for which it was not clear whether *XIST* was expressed from one or both alleles were included in the green category. Total of $n=42$ cells from 3 ovaries. **e**, Immuno-RNA FISH analysis of NANOG, DAZL and *XIST* RNA in week 14 p.f. ovaries (1 pair of ovaries). Scale bar, 30 μm. **f**, The proportion of cells with the indicated *XIST* expression patterns similar to in **c** in female hPGCs ($NANOG^+DAZL^+$) and meiotic germ cells ($NANOG^-DAZL^+$) from **e**. $n=104$ and $n=98$ cells, respectively from 1 sample. **g**, Female $NANOG^+$ pre-implantation epiblast (pre-Epi) and post-implantation epiblast (post-Epi) cells predominantly express *XACT* and *XIST* from both X chromosomes. Although genes on both X chromosomes in pre-implantation epiblast cells are dampened due to XCD (Xd)[14], it is unclear whether XCD also occurs in female post-implantation epiblast cells. However, expression of both *XACT* and *XIST* from both X chromosomes indicates that XCI has not yet occurred. $NANOG^+$ female hPGCs, similar to pre-implantation epiblast cells, exhibit XCD with expression of *XIST* and *XACT* from both alleles. Notably, *XIST* is more dispersed in the nucleus of hPGCs (shown by the glow around the X chromosome) compared with pre/post-implantation epiblast cells. After advancement to meiosis, female germ cells silence both *XIST* and *XACT* and upregulate X-linked gene expression, transitioning to the Xa state. Next, in primordial oocytes, the X/A ratio is reduced to lower than in female hPGCs without expression of *XIST*. We call this *XIST*-independent repression of the X/A ratio oocyte-specific X-chromosome regulation (X^O). Male hPGCs harbour an Xa but exhibit a lower X/A ratio compared with male somatic cells, and this state is retained after differentiation into prospermatogonia. We refer to this state as Xa*. Gonadal somatic cells display XCI at each stage analysed.

Although our imaging approaches demonstrated the presence of two active X chromosomes in female hPGCs, the scRNA-seq data revealed that the X/A ratio is reduced in female hPGCs compared with female meiotic germ cells (Fig. 6g). These results indicate that X-linked dosage compensation in female hPGCs is regulated by the XCD mechanism, similar to female naive human pluripotent stem cells[22] and female human pre-implantation embryos[14]. Although XCD is a transient state in pre-implantation embryos, in the case of hPGCs, we show that XCD is not a transitional state into XCI, but rather a stable state that lasts for at least 6 weeks until the point of meiotic initiation (Fig. 6g). Similar to female mouse PGCs[12], we also show that the X/A ratio excess occurs as female hPGCs initiate meiosis. After prophase I of meiosis I, the X/A ratio quickly declines coincident with primordial oocyte formation indicating a third unique state of X-chromosome dosage compensation, which we have called oocyte-specific X-chromosome regulation (X^O; Fig. 6g). Interestingly, the loss of XCD in the female germline after meiotic entry is linked to the silencing of *XIST* (Fig. 6g), suggesting that *XIST* is the mediator of XCD. By contrast, the further decline in the X/A ratio in primordial oocytes occurs in the absence of *XIST* expression. It remains unclear whether this regulation is achieved by XCD or other mechanisms.

Given that male hPGCs have a reduced X/A ratio compared with female and male somatic cells and female hPGCs, we refer to the active X chromosome in male prenatal germ cells as Xa* (Fig. 6g). The lower X/A ratio in male hPGCs relative to female hPGCs could be due to inefficient dampening of X-linked gene expression from both X chromosomes by *XIST* in female hPGCs, such that the levels in female hPGCs are higher than males. In support of this hypothesis, *XIST* is highly dispersed in female hPGCs, which may lead to less efficient XCD compared with the more cloud-like distribution of *XIST* reported for the pre-implantation embryo[14,15]. By contrast, a higher X/A ratio in female and male somatic cells could be explained by upregulation of single Xa in somatic cells[12,46,47], which may not occur in female or male hPGCs. Combined with XCD occurring on the X chromosomes in female hPGCs, this alternative explanation would explain the lower X-linked gene expression in female hPGCs compared with somatic cells.

As germline specification in humans takes days compared with hours in mice, and hPGC development is a much lengthier process than in mice, it is conceivable that the maintenance of X-chromosome dosage compensation in germ cells between the two species is different. It is probable that a primate-specific X-chromosome regulation mechanism might be necessary to compensate dosage of X-linked genes in the human embryo during PGC specification and the first trimester of pregnancy. However, how *XIST* and *XACT* contribute to X-chromosome gene regulation in the developing human germline will need to be studied mechanistically. Achieving this goal will require new in vitro cell models of hPGC development that have the ability to reliably promote the differentiation of hPGCLCs into meiotic germ cells and primordial oocytes combined with functional approaches[48].

X-chromosome dosage regulation might be extremely important for patients with Turner (XO) and Klinefelter (XXY) syndrome, who have infertility associated with loss of germline cells[49,50]. Although germline development in fetuses diagnosed with Turner syndrome is morphologically normal, oocyte loss occurs within the first few months after birth[51]. Potentially, meiosis does not occur correctly in patients with Turner syndrome due to diminished levels of critical X-linked genes in differentiating XO hPGCs compared with XX hPGCs. Thus, upregulation of X-linked gene expression with entrance into meiosis may be necessary for the formation of mature oocytes.

In summary, with the demonstration of XCD, our research draws parallels between the X-chromosome state of human epiblast and hPGCs. Our study sheds light on mechanisms that regulate X-linked gene expression in hPGCs before meiosis, and reveals a unique X-chromosome state in oocytes, which could potentially be important for oocyte formation and zygote development downstream.

Online content

Any methods, additional references, Nature Research reporting summaries, source data, extended data, supplementary information, acknowledgements, peer review information; details of author contributions and competing interests; and statements of data and code availability are available at https://doi.org/10.1038/s41556-020-00607-4.

Received: 24 February 2020; Accepted: 27 October 2020;
Published online: 30 November 2020

References

1. Deng, X., Berletch, J. B., Nguyen, D. K. & Disteche, C. M. X chromosome regulation: diverse patterns in development, tissues and disease. *Nat. Rev. Genet.* **15**, 367–378 (2014).
2. Payer, B. & Lee, J. T. X chromosome dosage compensation: how mammals keep the balance. *Annu. Rev. Genet.* **42**, 733–772 (2008).
3. Wutz, A. Gene silencing in X-chromosome inactivation: advances in understanding facultative heterochromatin formation. *Nat. Rev. Genet.* **12**, 542–553 (2011).
4. Gendrel, A.-V. & Heard, E. Fifty years of X-inactivation research. *Development* **138**, 5049–5055 (2011).
5. Plath, K., Mlynarczyk-Evans, S., Nusinow, D. A. & Panning, B. Xist RNA and the mechanism of X chromosome inactivation. *Annu. Rev. Genet.* **36**, 233–278 (2002).

6. Robert Finestra, T. & Gribnau, J. X chromosome inactivation: silencing, topology and reactivation. *Curr. Opin. Cell Biol.* **46**, 54–61 (2017).
7. Brockdorff, N. Localized accumulation of Xist RNA in X chromosome inactivation. *Open Biol.* **9**, 190213 (2020).
8. Sahakyan, A., Plath, K. & Rougeulle, C. Regulation of X-chromosome dosage compensation in human: mechanisms and model systems. *Philos. Trans. R. Soc. Lond. B* **372**, 20160363 (2017).
9. Chuva de Sousa Lopes, S. M. et al. X chromosome activity in mouse XX primordial germ cells. *PLoS Genet.* **4**, e30 (2008).
10. Sugimoto, M. & Abe, K. X chromosome reactivation initiates in nascent primordial germ cells in mice. *PLoS Genet.* **3**, 1309–1317 (2007).
11. de Napoles, M., Nesterova, T. & Brockdorff, N. Early loss of Xist RNA expression and inactive X chromosome associated chromatin modification in developing primordial germ cells. *PLoS ONE* **2**, e860 (2007).
12. Sangrithi, M. N. et al. Non-Canonical and sexually dimorphic X dosage compensation states in the mouse and human germline. *Dev. Cell* **40**, 289–301 (2017).
13. Nesterova, T. B. et al. Characterization of the genomic Xist locus in rodents reveals conservation of overall gene structure and tandem repeats but rapid evolution of unique sequence. *Genome Res.* **11**, 833–849 (2001).
14. Petropoulos, S. et al. Single-cell RNA-seq reveals lineage and X chromosome dynamics in human preimplantation embryos. *Cell* https://doi.org/10.1016/j.cell.2016.03.023 (2016).
15. Okamoto, I. et al. Eutherian mammals use diverse strategies to initiate X-chromosome inactivation during development. *Nature* **472**, 370–374 (2011).
16. Moreira de Mello, J. C. et al. Random X inactivation and extensive mosaicism in human placenta revealed by analysis of allele-specific gene expression along the X chromosome. *PLoS ONE* **5**, e10947 (2010).
17. Vallot, C. et al. XACT noncoding RNA competes with XIST in the control of X chromosome activity during human early development. *Cell Stem Cell* **20**, 102–111 (2017).
18. Vallot, C. et al. *XACT*, a long noncoding transcript coating the active X chromosome in human pluripotent cells. *Nat. Genet.* **45**, 239–241 (2013).
19. Patrat, C., Ouimette, J.-F. & Rougeulle, C. X chromosome inactivation in human development. *Development* **147**, dev183095 (2020).
20. Moreira de Mello, J. C., Fernandes, G. R., Vibranovski, M. D. & Pereira, L. V. Early X chromosome inactivation during human preimplantation development revealed by single-cell RNA-sequencing. *Sci. Rep.* **7**, 10794 (2017).
21. Sousa, E. J. et al. Exit from naive pluripotency induces a transient X chromosome Inactivation-like state in males. *Cell Stem Cell* **22**, 919–928 (2018).
22. Sahakyan, A. et al. Human naive pluripotent stem cells model X chromosome dampening and X inactivation. *Cell Stem Cell* **20**, 87–101 (2016).
23. Patel, S. et al. Human embryonic stem cells do not change their X inactivation status during differentiation. *Cell Rep.* **18**, 54–67 (2016).
24. Tang, W. W. C. et al. A unique gene regulatory network resets the human germline epigenome for development. *Cell* **161**, 1453–1467 (2015).
25. Gkountela, S. et al. DNA demethylation dynamics in the human prenatal germline. *Cell* **161**, 1425–1436 (2015).
26. Guo, F. et al. The transcriptome and DNA methylome landscapes of human primordial germ cells. *Cell* **161**, 1437–1452 (2015).
27. Anderson, R. A., Fulton, N., Cowan, G., Coutts, S. & Saunders, P. T. K. Conserved and divergent patterns of expression of DAZL, VASA and OCT4 in the germ cells of the human fetal ovary and testis. *BMC Dev. Biol.* **7**, 136 (2007).
28. Gkountela, S. et al. The ontogeny of cKIT$^+$ human primordial germ cells proves to be a resource for human germ line reprogramming, imprint erasure and in vitro differentiation. *Nat. Cell Biol.* **15**, 113–122 (2012).
29. Perrett, R. M. et al. The early human germ cell lineage does not express SOX2 during in vivo development or upon in vitro culture. *Biol. Reprod.* **78**, 852–858 (2008).
30. Vértesy, Á. et al. Parental haplotype-specific single-cell transcriptomics reveal incomplete epigenetic reprogramming in human female germ cells. *Nat. Commun.* **9**, 1873 (2018).
31. Plath, K. et al. Role of histone H3 lysine 27 methylation in X inactivation. *Science* **300**, 131–135 (2003).
32. Silva, J. et al. Establishment of histone H3 methylation on the inactive X chromosome requires transient recruitment of Eed-Enx1 polycomb group complexes. *Dev. Cell* **4**, 481–495 (2003).
33. Chen, D. et al. The TFAP2C-regulated *OCT4* naive enhancer is involved in human germline formation. *Cell Rep.* **25**, 3591–3602 (2018).
34. Kobayashi, T. & Surani, M. A. On the origin of the human germline. *Development* **145**, dev150433 (2018).
35. Sasaki, K. et al. Robust in vitro induction of human germ cell fate from pluripotent stem cells. *Cell Stem Cell* **17**, 178–194 (2015).
36. Diaz Perez, S. V. et al. Derivation of new human embryonic stem cell lines reveals rapid epigenetic progression in vitro that can be prevented by chemical modification of chromatin. *Hum. Mol. Genet.* **21**, 751–764 (2011).
37. Pandolfi, E. C. et al. Generation of three human induced pluripotent stem cell sublines (MZT04D, MZT04J, MZT04C) for reproductive science research. *Stem Cell Res.* **40**, 101576 (2019).
38. Deglincerti, A. et al. Self-organization of the in vitro attached human embryo. *Nature* **533**, 251–254 (2016).
39. Shahbazi, M. N. et al. Self-organization of the human embryo in the absence of maternal tissues. *Nat. Cell Biol.* **18**, 700–708 (2016).
40. Li, L. et al. Single-cell RNA-seq analysis maps development of human germline cells and gonadal niche interactions. *Cell Stem Cell* 858–873 (2017); https://doi.org/10.1016/j.stem.2017.03.007
41. Wolf, F. A. et al. PAGA: graph abstraction reconciles clustering with trajectory inference through a topology preserving map of single cells. *Genome Biol.* **20**, 59 (2019).
42. Anderson, E. L. et al. Stra8 and its inducer, retinoic acid, regulate meiotic initiation in both spermatogenesis and oogenesis in mice. *Proc. Natl Acad. Sci. USA* **105**, 14976–14980 (2008).
43. Törmälä, R. M. et al. Zona pellucida components are present in human fetal ovary before follicle formation. *Mol. Cell. Endocrinol.* **289**, 10–15 (2008).
44. Zhang, Y. et al. Transcriptome landscape of human folliculogenesis reveals oocyte and granulosa cell interactions. *Mol. Cell* **72**, 1021–1034 (2018).
45. Casanova, M. et al. A primate-specific retroviral enhancer wires the XACT lncRNA into the core pluripotency network in humans. *Nat. Commun.* **10**, 5652 (2019).
46. Larsson, A. J. M., Coucoravas, C., Sandberg, R. & Reinius, B. X-chromosome upregulation is driven by increased burst frequency. *Nat. Struct. Mol. Biol.* **26**, 963–969 (2019).
47. Deng, X. et al. Evidence for compensatory upregulation of expressed X-linked genes in mammals, *Caenorhabditis elegans* and *Drosophila melanogaster*. *Nat. Genet.* **43**, 1179–1185 (2011).
48. Yamashiro, C. et al. Generation of human oogonia from induced pluripotent stem cells in vitro. *Science* **362**, 356–360 (2018).
49. Folsom, L. J. & Fuqua, J. S. Reproductive issues in women with Turner syndrome. *Endocrinol. Metab. Clin. North Am.* **44**, 723–737 (2015).
50. Franik, S. et al. Klinefelter syndrome and fertility—impact of X-chromosomal inheritance on spermatogenesis. *Andrologia* **50**, e13004 (2018).
51. Reynaud, K. et al. Number of ovarian follicles in human fetuses with the 45,X karyotype. *Fertil. Steril.* **81**, 1112–1119 (2004).
52. Irie, N. et al. SOX17 is a critical specifier of human primordial germ cell fate. *Cell* **160**, 253–268 (2015).
53. Chen, D. et al. Germline competency of human embryonic stem cells depends on eomesodermin. *Biol. Reprod.* **97**, 850–861 (2017).

Methods

Human fetal tissues. Prenatal gonads (4–16 weeks p.f.) were obtained from either the University of Washington Birth Defects Research Laboratory (BDRL) or the University of Tubingen. At the BDRL, prenatal gonads were obtained with regulatory oversight from the University of Washington IRB approved Human Participants protocol, combined with a Certificate of Confidentiality from the Federal Government. BDRL collected the fetal testes and ovaries and shipped them overnight in HBSS with an ice pack for immediate processing at UCLA. Prenatal samples from the University of Tübingen were delivered to UCLA 24–48 h after the procedure. The research project was also approved by the research ethics committee of the University of Tübingen (IRB, 584/2018BO2 and 634/2017BO1). All human fetal tissue used here was obtained following informed consent. The donated human fetal tissue sent to UCLA did not carry any personal identifiers. No payments were made to donors and the donors knowingly and willingly consented to provide research materials without restrictions for research and for use without identifiers. Developmental age was documented by the BDRL and the University of Tübingen as days p.f. using a combination of prenatal intakes and Carnegie staging. A total of 16 fetal samples was used for this study.

Human pre-implantation embryos. The use of human embryos in this research project followed California State law and was reviewed by the Institutional Review Board (IRB) and the human embryonic stem cell research oversight committee (ESCRO) at UCLA. The ESCRO committee at UCLA approves human pluripotent stem cell and human embryo work at UCLA according to 2016 ISSCR guidelines. Together, these committees approve the process of informed consent, and experiments using human embryos for research purposes on an annual basis. Patients were not paid for participating, and all of the donors were informed that the embryos would be destroyed as part of the research study. All research in this study using human embryos complied with the principles that are laid out in the International Society for Stem Cell Research. Frozen human blastocysts at days 6–7 p.f. were used in this study and thawed using the Vit Kit-Thaw (Irvine Scientific) according to manufacturer's protocol. After thawing, embryos were cultured overnight in 5% O_2, 6% CO_2 at 37 °C, and the zona pellucida was removed with Tyrode's acidified solution (Irvine Scientific). A total of 28 human blastocysts were used here. The sex of the blastocysts was determined by cloud counts of lncRNA *XIST* and *XACT* expression from a single (male) or both X chromosomes (female).

Tissue processing for scRNA-seq. Fetal tissues were processed 24–48 h after termination. On arrival, tissues were gently washed with PBS and placed in dissociation buffer containing of collagenase IV 10 mg ml^{-1} (Life Technologies, 17104-019), dispase II 250 µg ml^{-1} (Life Technologies, 17105041), DNase I 1:1,000 (Sigma-Aldrich, 4716728001), 10% fetal bovine serum (Life Technologies, 10099141) in 1× PBS. Tissues were dissociated for 15 min at 37 °C. After every 5 min, the tissues were pipetted against the bottom of Eppendorf tube. Cells were subsequently centrifuged for 5 min at 500*g*, resuspended in 1× PBS with 0.04% BSA, strained through a 40 µm strainer and counted using an automated cell counter (Thermo Fisher Scientific, Countess II). The cell concentration was adjusted to 800–1,200 cells per µl and immediately used for scRNA-seq.

scRNA-seq library preparation and sequencing. scRNA-seq libraries were generated using the 10x Genomics Chromium instrument and Chromium Single Cell 3′ Reagent Kit v2. Each individual library was designed to target 6,000 cells. Libraries were generated according to the manufacturer's instructions and library fragment size distribution was determined using a BioAnalyzer instrument. Libraries were pooled together and sequenced using an Illumina Novaseq 6000 platform, at an average depth of 400–420 million reads per sample.

scRNA-seq data analysis. scRNA-seq reads were aligned to the human hg38 genome assembly using 10x Genomics Cell ranger v.2.2. Expression matrixes generated by Cell Ranger were imported into Scanpy[54] for downstream analysis. First, all of the libraries were merged, and cells were filtered in the same manner. All of the genes that were expressed in less than five cells were discarded and cells with less than 250 detected genes were filtered out. The unique molecular identifier (UMI) counts were then normalized for each cell by the total expression, multiplied by 10,000 and log-transformed. Using Scanpy's default method, highly variable genes were identified, and data were scaled to regress out variation from UMI counts and mitochondrial genes. Cells were clustered using the Louvain algorithm[55] and the UMAP package was used to visualize cells in a two-dimensional plot[54]. Germ cell clusters were identified by expression of germ-cell-specific markers, such as *NANOS3*, *DAZL*, *DDX4* and *SYCP1*. Gonadal somatic cells were annotated by previously published literature[40]. The female and male germline trajectories were created by partition-based graph abstraction[41]. The dataset of Li at al.[40] was analysed through the same pipeline as described above. Gene expression matrixes of female and male germ cells were exported from Scanpy and X/A ratio per cell were calculated using a custom R script.

Tissue processing and cryo-sectioning. On arrival, fetal tissues were gently washed with 1× PBS and fixed with freshly made 4% paraformaldehyde in 1× PBS for 3–4 h on a rotator at room temperature. Tissues were washed with 1× PBS three times for 5 min and moved through increasing concentrations of sucrose—10% sucrose for 1 h, 20% for 1 h and 30% overnight at 4 °C. Tissues were next embedded in O.C.T. (Tissue-Tek) and sections (7 µm) were cut. Sections and tissue blocks were kept at −80 °C.

hESC culture. The hESC and hiPSC lines used in this study include UCLA2 (46, XY)[36] and MZTO4 iPSC (46, XX)[37]. hESCs and hiPSCs were cultured on mitomycin-C-inactivated mouse embryonic fibroblasts (MEFs) in hESC medium, which is composed of 20% knockout serum replacement (KSR) (GIBCO, 10828-028), 100 mM L-glutamine (GIBCO, 25030-081), 1× MEM non-essential amino acids (NEAA) (GIBCO, 11140-050), 55 mM 2-mercaptoethanol (GIBCO, 21985-023), 10 ng ml^{-1} recombinant human FGF basic (R&D systems, 233-FB), 1× penicillin–streptomycin (GIBCO, 15140-122) and 50 ng ml^{-1} primocin (InvivoGen, ant-pm-2) in DMEM/F12 medium (GIBCO, 11330-032). The hESCs and iPSCs were split every 7–8 d using collagenase type IV (GIBCO, 17104-019). The hESC line used in this study is registered with the National Institute of Health Human Embryonic Stem Cell Registry and available for research use with NIH funds. Mycoplasma tests (Lonza, LT07-418) were performed every month for all cell lines used in this study. All of the experiments were approved by the UCLA ESCRO Committee.

hPGCLC differentiation. hPGCLCs were induced from primed hESCs and hiPSCs as described previously[53] with stem cell factor omitted from the differentiation medium and starting with human pluripotent stem cells grown on MEFs. In brief, hESCs and hiPSCs were dissociated into single cells with 0.05% trypsin-EDTA (GIBCO, 25300-054) and plated onto human-plasma-derived fibronectin-coated (Invitrogen, 33016-015) 12-well plates at a density of 200,000 cells per well in 2 ml per well of iMeLC medium (15% KSR (GIBCO, 10828-028), 1× NEAA (GIBCO, 11140-050), 0.1 mM 2-mercaptoethanol (GIBCO, 21985-023), 1× penicillin–streptomycin–glutamine (GIBCO, 10378-016), 1 mM sodium pyruvate (GIBCO, 11360-070), 50 ng ml^{-1} activin A (Peprotech, AF-120-14E), 3 mM CHIR99021 (Stemgent, 04-0004), 10 mM of ROCKi (Y27632, Stemgent, 04-0012-10) and 50 ng ml^{-1} primocin in Glasgow's MEM (GMEM) (GIBCO, 11710-035)). After 24 h, iMeLCs were dissociated into single cells with 0.05% trypsin-EDTA and plated into ultra-low cell attachment U-bottom 96-well plates (Corning, 7007) at a density of 3,000 cells per well in 200 ml per well of hPGCLC medium, which is composed of 15% KSR (GIBCO, 10828-028), 1× NEAA (GIBCO, 11140-050), 0.1 mM 2-mercaptoethanol (GIBCO, 21985-023), 1× penicillin–streptomycin-–glutamine (GIBCO, 10378-016), 1 mM sodium pyruvate (GIBCO, 11360-070), 10 ng per ml^{-1} human LIF (Millipore, LIF1005), 200 ng ml^{-1} human BMP4 (R&D systems, 314-BP), 50 ng ml^{-1} human EGF (R&D systems, 236-EG), 10 mM of ROCKi (Y27632, Stemgent, 04-0012-10) and 50 ng ml^{-1} primocin in GMEM (GIBCO, 11710-035).

hPGCLC sorting and preparation for RNA FISH. hPGCLC aggregates were dissociated 0.05% trypsin-EDTA (GIBCO, 25300-054) for 10 min at 37 °C. The dissociated cells were stained with conjugated antibodies, washed with FACS buffer (1% BSA in PBS) and resuspended in FACS buffer with 7-AAD (BD PharMingen, 559925) as viability dye. The conjugated antibodies used in this study include ITGA6 conjugated with BV421 (BioLegend, 313624, 1:60), EPCAM conjugated with 488 (BioLegend, 324210, 1:60). The single-cell suspension was sorted for further experiments using BD FACSAria FACS machine. FACS data were analysed using FlowJo v.10. Double-positive cells for ITGA6 and EPCAM (hPGCLCs) and negative cells (non-hPGCLCs) were collected in hPGCLC medium and plated on human-plasma-derived fibronectin-coated coverslips overnight. The next morning, RNA FISH was performed using the coverslips.

Immunofluorescence. Slides of paraffin-embedded sections were deparaffinized by successive treatment with xylene and 100%, 95%, 70% and 50% ethanol. Antigen retrieval was performed by incubation with 10 mM Tris pH 9.0, 1 mM EDTA, 0.05% Tween-20 at 95 °C for 40 min. The slides were cooled and washed with 1× PBS and 1× TBS (PBS + 0.2% Tween-20). Cryosections and blastocysts attached to Ibidi chambers were fixed with 4% PFA for 10 min and then washed with 1× PBS. Paraffin-embedded sections, cryosections and blastocysts were treated similarly. The samples were permeabilized with 0.5% Triton X-100 in 1× PBS, then washed with 1× TBS and blocked with 1% BSA in 1× TBS. Primary antibody incubation was conducted with 1% BSA for 1 h at room temperature. Samples were again washed with 3× TBS-Tween-20 and incubated with fluorescent secondary antibodies at 1:200 for 45 min, then washed and counterstained with DAPI for 5 min and mounted using Vectashield. A list of the primary antibodies used for immunofluorescence in this study is provided in Supplementary Table 1 under the antibody list tab. The secondary antibodies used in this study were all obtained from Life technologies and were used at 1:400 dilution. Images were taken using a LSM 880 Confocal Instrument (Zeiss) or Zeiss Axio Imager M1. For image processing and analysis, Fiji (ImageJ) was used. For signal quantification, images were converted into 8-bit images and then analysed using profile plot tool. Intensity values were exported as a CSV file and then R Studio and the ggplot2 package was used for plotting.

RNA FISH. After sorting, hPGCLCs and non-hPGCLCs were attached to fibronectin-coated 18 mm circular glass coverslips (Thermo Fisher Scientific, 12-545-100) overnight. The next morning, the coverslips were washed with DPBS, fixed with 4% formaldehyde for 10 min, permeabilized with cold (4 °C) 0.5% Triton X-100 in DPBS for 10 min and serially dehydrated with cold (4 °C) 70–100% ethanol. Coverslips were air dried and hybridized with labelled DNA probes in a humidified chamber at 37 °C overnight, washed for three 5 min intervals with 50% formamide in 2× SSC, 2× SSC, then 1× SSC at 42 °C, counterstained with DAPI and mounted with Vectashield (Vector Labs, H-1000). Double-stranded DNA probes were generated from full-length cDNA constructs or bacterial artificial chromosomes (BACs) as described previously[56]. The following BACs were used: *XIST* (RP11-13M9), *XACT* (RP11-35D3), *ATRX* (RP11-1145J4) and *HUWE1* (RP11-975N19). Every new batch of probes was tested on normal human dermal fibroblasts before it was used in experiments.

Immuno-RNA FISH. Immuno-RNA FISH on cryosections was performed as described previously described[56]. In brief, immunostaining was performed first on cryosections and blastocysts as described above. Samples were post-fixed with 4% PFA after immunofluorescence staining, and RNA FISH was performed after post-fixation as described in RNA FISH section above.

Immuno-RNA FISH analysis of human blastocysts was performed as described previously[23] with the following modifications: embryos at day 5 and day 6 p.f. were thawed for these experiments and cultured for 24 h before staining. First, zona pellucida was removed with Tyrode's acid and blastocysts were washed with 6 mg ml^{-1} BSA (Sigma-Aldrich) in RNase–DNase-free PBS. Blastocysts were then individually transferred to Ibidi chambers (Ibidi, 80827), which were coated with polylysine (Sigma-Aldrich, P4832-50ML). Fluid was aspirated until dry and the blastocysts were fixed with ice-cold 4% paraformaldehyde (PFA) for 10 min at room temperature. Immunostaining was performed as described above. In all buffers and antibody solutions, RNaseOUT 1:200 (Thermo Fisher Scientific, 10777019) was added to preserve RNA. Before performing RNA FISH, samples were post-fixed with 4% PFA for 10 min at room temperature. RNA FISH was then performed using DNA probes as described above.

Attached blastocyst culture. Human embryo attachment culture was performed according to previously described procedures[38,39]. In brief, cryopreserved human blastocysts were received vitrified from the IVF clinic following consent and thawed using Vit Kit-Thaw (Irvine Scientific) according to manufacturer's protocol. The embryos were cultured in drops of Continuous Single Culture Complete medium, which was presupplemented with HSA (Irvine Scientific) under mineral oil (Irvine Scientific) overnight at 37 °C, 6% CO_2 and 5% O_2. The zona pellucida was removed using Tyrode's solution acidified (Irvine Scientific) and plated onto an m-Slide eight-well chamber slide (Ibidi) in IVC-1 medium (Cell Guidance Systems) and incubated for 2 d at 37 °C and 5% CO_2 to allow for attachment. Medium was half replaced on the second and third day with IVC-1. From the fourth day onward, the medium was completely replaced with IVC-2 medium (Cell Guidance Systems) until the appropriate developmental day was reached up to a maximum of day 12, which includes the blastocyst stage plus days in culture. For these experiments, 9 blastocysts were cultured up to day 12 p.f., out of which 5 were used for immuno-RNA FISH experiments.

Bulk RNA-seq data analysis. Published raw population RNA-seq datasets[25,52,53] of male and female hPGCs and somatic cells were downloaded and realigned to the hg19 genome as described previously[17] for lncRNA *XACT* expression analysis. Expression tracks were generated using pyGenomeTracks package[57].

Statistics and reproducibility. In the quantitative data, significance was assessed using Wilcoxon tests; *$P<0.05$, **$P<0.01$, ***$P<0.001$; ns, non-significant. Statistical analyses are described in detail in the figure legends for each panel. Immuno-RNA FISH experiments were performed in two independent experiments with similar results, unless specified otherwise in the legends. scRNA-seq datasets were pooled from ten independent experiments. No statistical methods were used to predetermine the sample size; rather, sample size was limited by the availability of prenatal tissues. Signal intensity measurement details are described in the Immunofluorescence section. For plotting and statistical analysis of scRNA-seq datasets and immune-RNA FISH quantifications, ggsignif and ggplot2 R packages were used.

Reporting Summary. Further information on research design is available in the Nature Research Reporting Summary linked to this article.

Data availability

The scRNA-seq data of prenatal tissues reported in this paper are available under the following accession numbers: GSE143380 (female cell data) and GSE143356 (male cell data). scRNA-seq datasets are also available online for interactive exploration (http://germline.mcdb.ucla.edu). Previously published RNA-seq data of male and female hPGCs and somatic cells[25,52,53] and single-cell RNA-seq data from female germ cells[30] and from female FCGs[40] that were reanalysed here are available under the following accession codes: GSE63392 (ref. [25]), GSE60138 (ref. [52]), GSE93126 (ref. [53]), GSE79280 (ref. [30]) and GSE86146 (ref. [40]), respectively. Human conceptus tissue requests can be made to bdrl@u.washington.edu. All other data supporting the findings of this study are available from the corresponding authors on reasonable request. Source data are provided with this paper.

Code availability

Custom scripts used for aligning population RNA-seq, scRNA-seq, data processing and plotting are available on request.

References

54. Wolf, F. A., Angerer, P. & Theis, F. J. SCANPY: large-scale single-cell gene expression data analysis. *Genome Biol.* **19**, 15 (2018).
55. Blondel, V. D., Guillaume, J.-L., Lambiotte, R. & Lefebvre, E. Fast unfolding of communities in large networks. *J. Stat. Mech. Theory Exp.* **2008**, P10008 (2008).
56. Solovei, I. Fluorescence in situ hybridization (FISH) on tissue cryosections. *Methods Mol. Biol.* **659**, 71–82 (2010).
57. Ramírez, F. et al. High-resolution TADs reveal DNA sequences underlying genome organization in flies. *Nat. Commun.* **9**, 189 (2018).

Acknowledgements

We thank J. Scholes, F. Codrea and J. Calimlim for support with FACS; J. Tang for banking and culturing of the UCLA hESC lines; staff at the microscopy cores at the UCLA Eli and Edythe Broad Center of Regenerative Medicine and Stem Cell Research Center (BSCRC) for help with imaging; staff at the Technology Center for Genomics and Bioinformatics at the UCLA Johnson Comprehensive Cancer Center (JCCC) and the Next Generation Sequencing core at BSCRC for help with genomics approaches; and staff at the Translational Pathology Core Laboratory for help with histology. T.C. was supported by a Boehringer Ingelheim PhD Fellowship. This work is supported by funds from the NIH to A.C. (R01HD079546). K.P. was supported by the BSCRC at UCLA, the David Geffen School of Medicine at UCLA, and the UCLA JCCC, the NIH (R01HD098387, P01GM099134) and a Faculty Scholar grant from the Howard Hughes Medical Institute. All human pre-implantation embryo and human embryo attachment culture studies were performed using funds from the UCLA Eli and Edythe Broad Center of Regenerative Medicine and Stem Cell Research Innovation Award. No NIH funds were used for research with human pre-implantation embryos. Human fetal tissue research is supported by a grant to I. Glass at the University of Washington Birth Defects laboratory (5R24HD000836-53).

Author contributions

T.C., K.P. and A.C. designed the experiments. T.C. and R.C. conducted immuno-RNA FISH experiments on tissues and in vitro PSC-derived cells. T.C., R.K. and E.P. generated female hiPSC lines from fibroblasts and conducted human blastocyst experiments. D.C. contributed to hPGCLC differentiation experiments. F.-M.H. created an interactive web-site to explore our scRNA-seq datasets. S.L. and K.S.-L. provided the human fetal tissues. T.C. performed scRNA-seq experiments, and the resulting data were analysed by T.C and I.D.; T.C analysed bulk RNA-seq data. T.C., K.P. and A.C. interpreted all data and wrote the manuscript.

Competing interests

The authors declare no competing interests.

Additional information

Extended data is available for this paper at https://doi.org/10.1038/s41556-020-00607-4.

Supplementary information is available for this paper at https://doi.org/10.1038/s41556-020-00607-4.

Correspondence and requests for materials should be addressed to K.P. or A.C.

Peer review information: Peer reviewer reports are available.

Reprints and permissions information is available at www.nature.com/reprints.

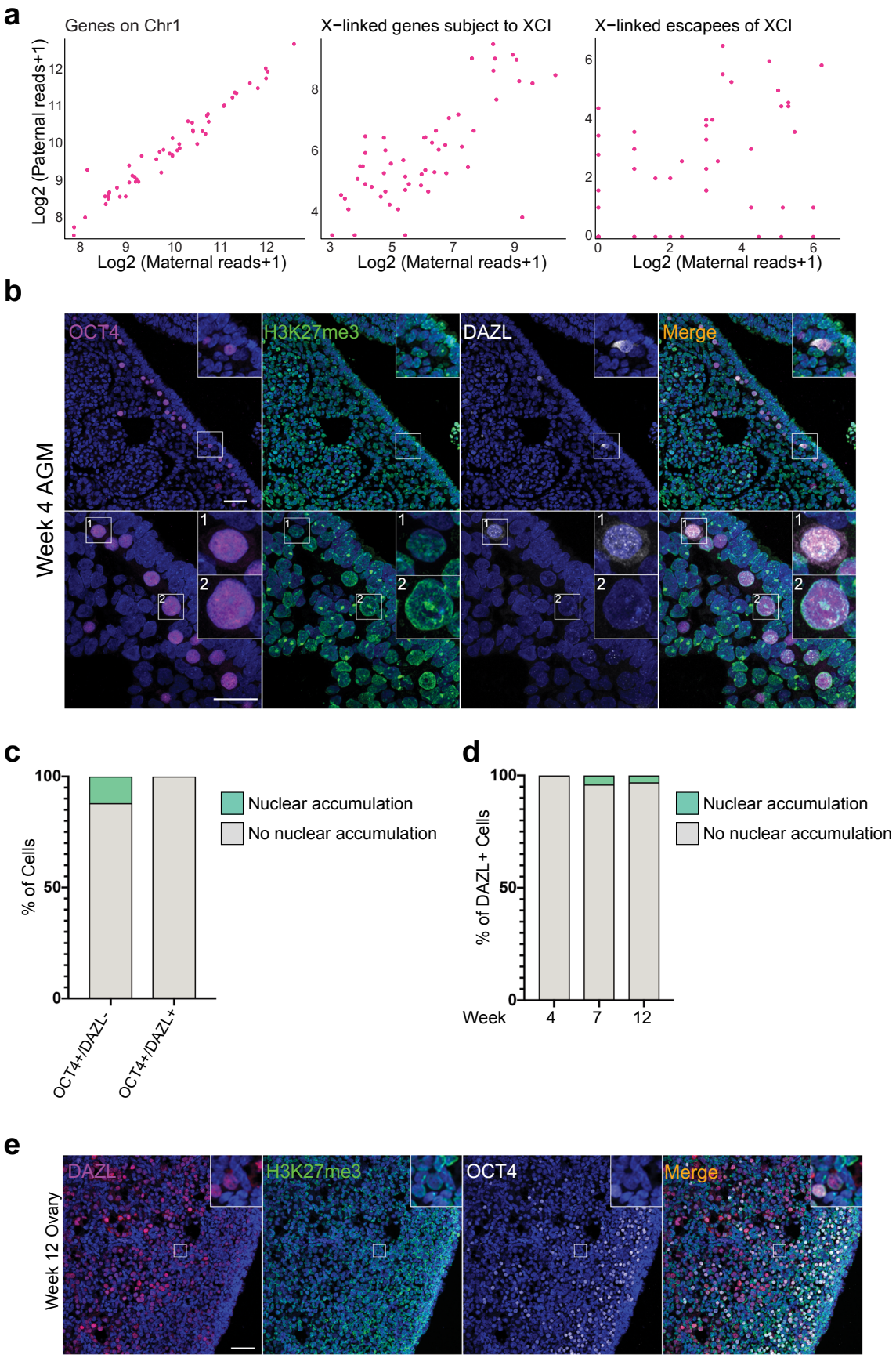

Extended Data Fig. 1 | See next page for caption.

Extended Data Fig. 1 | Female hPGCs from week 4 pf ovaries have lost the H3K27me3 nuclear accumulation. a, Distribution of single nucleotide polymorphisms (SNPs) from maternally inherited (x-axis) and paternally inherited (y-axis) alleles in gene expression data of female hPGCs. Each dot represents sum of all detected SNPs per cell for genes on chromosome 1 (Chr1), X-linked genes subject to XCI and escapees of XCI, respectively, based on published scRNA-seq data[30]. **b**, Representative immunofluorescence staining of OCT4 (magenta), H3K27me3 (green), DAZL (grey) and DAPI (blue) on female hPGCs at week 4 pf prior to gonad formation, when hPGCs are migrating through the aorta-gonad-mesonephros (AGM) (1 sample was analyzed). Insets show a rare OCT4+/DAZL+ cell with no nuclear accumulation of H3K27me3 (inset 1) and an OCT4+/DAZL- cell with H3K27me3 accumulation (inset 2) along the genital ridge of the AGM. Scale bar upper panel 50 microns, lower panel 30 microns. **c**, Percentage of OCT4+/DAZL+ and OCT4+/DAZL- cells with an Xi-like nuclear accumulation of H3K27me3 from the experiment shown in (**c**); (n=58 cells from 1 AGM). **d**, Quantification of the proportion of DAZL+ female hPGCs at weeks 4, 7 and 12 pf with an Xi-like nuclear accumulation of H3K27me3 (n=50-100 cells per sample in 2 replicates). **e**, Representative immunofluorescence staining of a fetal ovary at week 12 pf with DAZL (magenta), H3K27me3 (green), OCT4 (grey) and DAPI (blue). Inset shows a DAZL+/OCT4 negative female germ cell that is negative for H3K27me3 (1 pair of ovaries were analyzed), scale bar 50 microns. Statistical source data are provided in Source Data Extended Data Fig. 1.

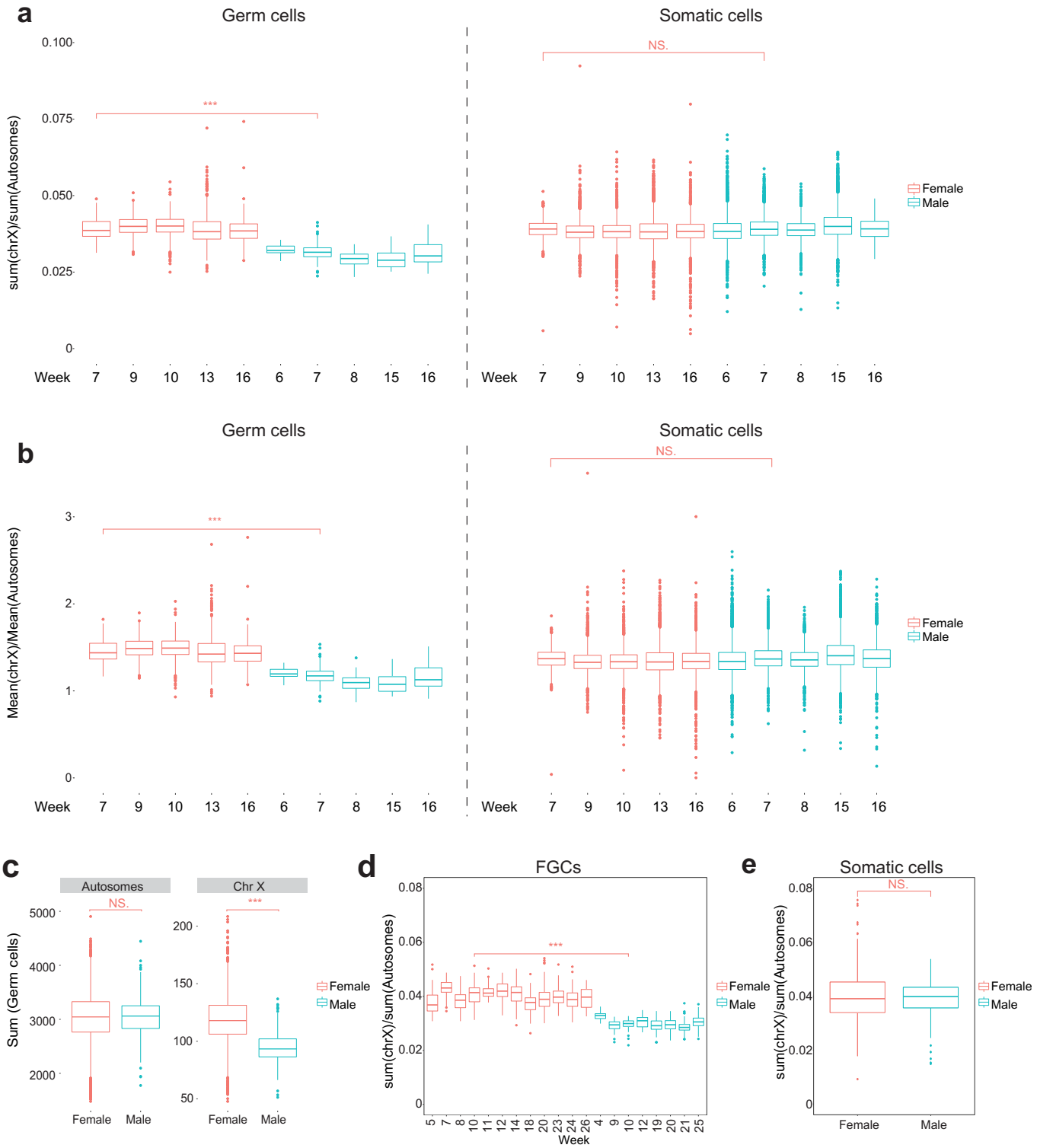

Extended Data Fig. 2 | The X/A ratio is higher in female germ cells than in male germ cells. a, Boxplots presenting the X/A ratio, calculated from the sum of X-linked linked gene expression and the sum of autosomal gene expression, of individual female (red) or male (cyan) germ cells (left panel) and surrounding somatic cells (right panel) obtained from gonads harvested from indicated developmental timepoints (week). **b**, As in (**a**), except that the X/A ratio was determined from the mean expression levels of X-linked and autosomal genes per cell. **c**, Boxplot showing the distribution of the sum of all autosomal (left) and X-linked (right) gene expression, respectively, in individual female and male germ cells across for developmental time points shown in (**a**). **d**, As in (**a**), except that the X/A ratios in female and male FGCs across developmental time from a published study are shown[40]. **e**, X/A ratio per single cell in female and male gonadal somatic cells from all developmental ages accompanying the data shown in (**d**). Wilcoxon statistical testing between age matched samples, NS- Not Significant, * p<0.05, ** p<0.01, *** p<0.001. a-c: n = 49528 cells analyzed across 10 independent experiments and d-e: 1016 cells analyzed from published dataset[40] in total.

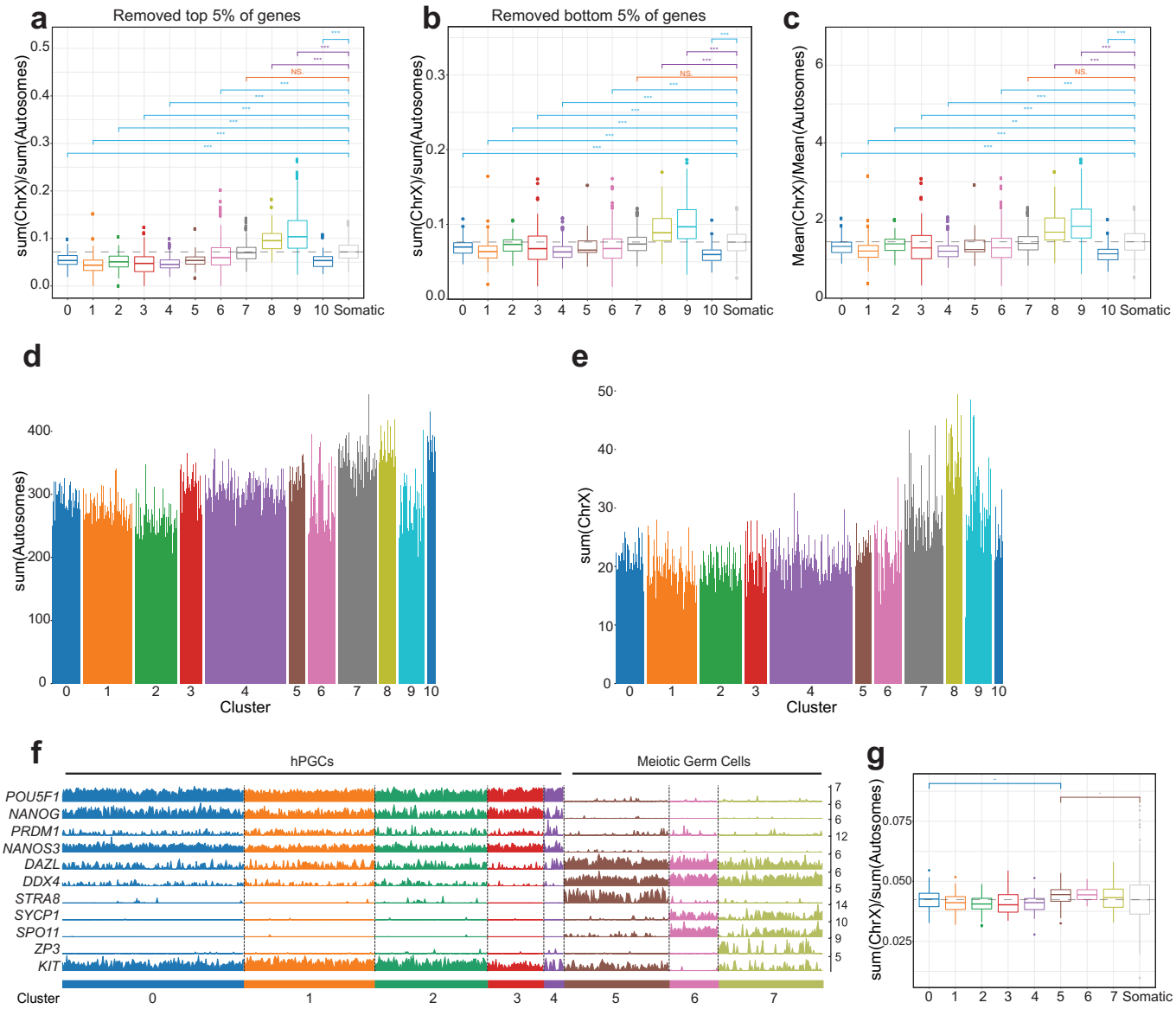

Extended Data Fig. 3 | Female hPGCs dampen X linked gene expression before entering meiosis. a, Boxplots of the X/A ratios of female germ cells along the developmental trajectory and in female gonadal somatic cells, as described in Fig. 5, except that the top 5% highest expressed genes were excluded from the analysis. **b**, As in (**a**), except that the bottom 5% of expressed genes were excluded from the analysis. **c**, Boxplots of the X/A ratios in female germ cells and female gonadal cells as described in Fig. 5, except that the X/A ratios were calculated from the mean value of X-linked and autosomal gene expression per cell. **d**, Sum of all autosomal gene expression normalized counts in female germ cells organized by clusters along the developmental trajectory. **e**, Sum of all X-linked gene expression in female germ cells organized by clusters along the developmental trajectory. X-linked gene expression increases in clusters 7-9 coincident with entrance into meiosis and repression of the naïve-like pluripotency program. **f**, Germline trajectory analysis of previously published scRNA-seq data from female FCGs[40]. The hPGCs state with pluripotency program expression is captured with clusters 0-4, and meiotic entry in cluster 5-7. **g**, Boxplots of the X/A ratios for female germ cells and female gonadal somatic cells for the data set shown in (**f**). From cluster 5 onwards, X/A ratios in differentiating female germ cells are higher than gonadal somatic cells. Wilcoxon statistical testing for (**a**), (**b**), (**c**), (**g**). NS- Not Significant, * p<0.05, ** p<0.01, *** p<0.001.

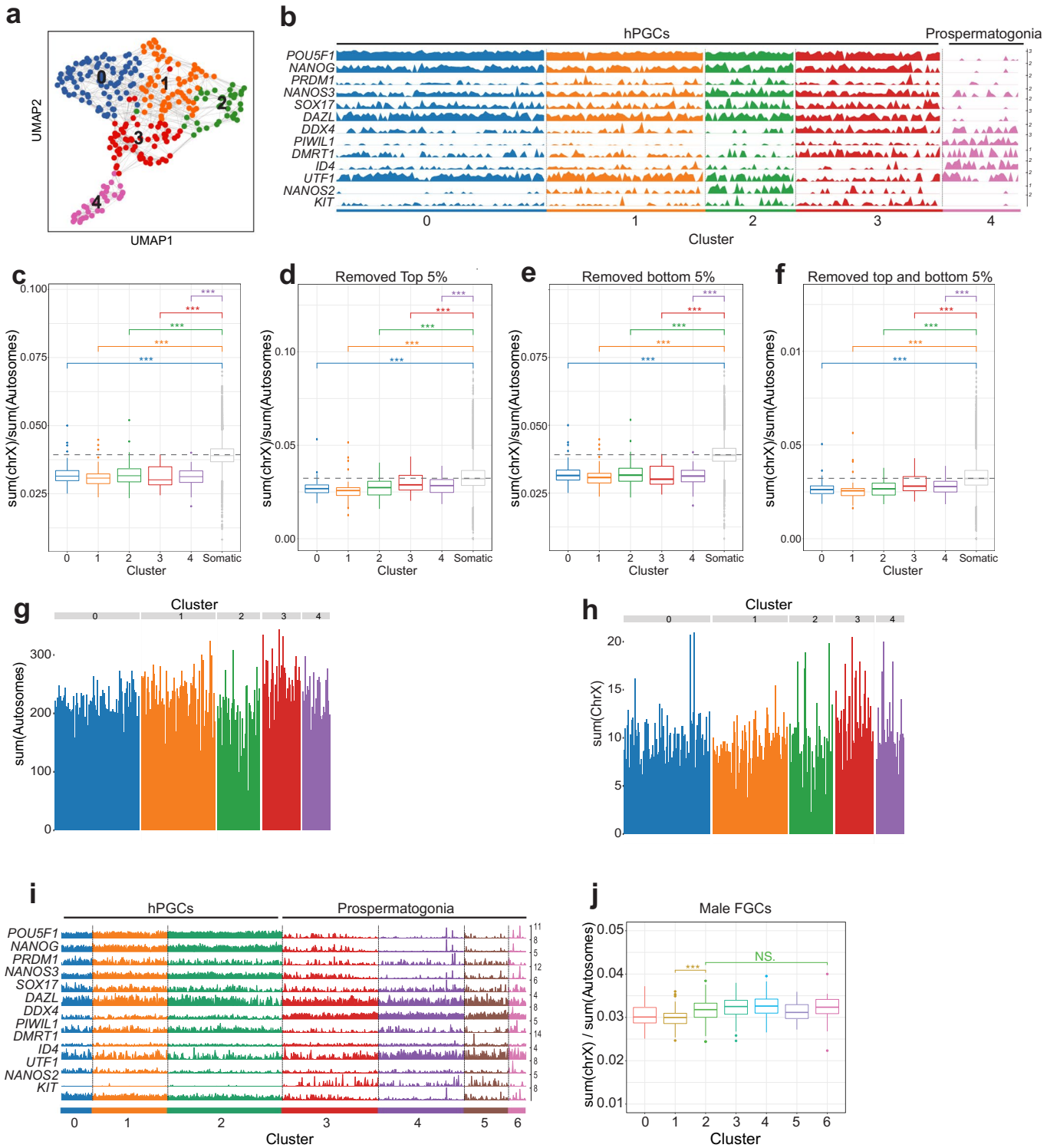

Extended Data Fig. 4 | See next page for caption.

Extended Data Fig. 4 | Male hPGCs do not change X/A ratio upon sex specific differentiation. a, Male germ cells from the scRNA-seq data shown in Fig. 4a–c were projected along the developmental trajectory, and five clusters (0-4) were identified (n= 282 cells pulled from 5 samples). The pluripotency program is repressed in cluster 4, coincident with increased expression of prospermatogonia genes and exit from the cell cycle. **b**, Expression of marker genes along the developmental trajectory of male germ cells defined in (**a**). **c**, Box plots showing that X/A ratios in male germ cells along the developmental trajectory and in surrounding male somatic cells. **d**, As in (**c**), except that the top 5% highest expressed genes were excluded from the analysis. **e**, As in (**c**), except that bottom 5% of genes were excluded. **f**, As in (**c**), except that the top and bottom 5% of expressed genes were excluded. In total n = 24740 cells analyzed across 5 independent experiments in **c**-**f**. **g**, Sum of all autosomal gene expression per cell in male germ cells along the developmental trajectory, showing no dramatic differences across the clusters. **h**, As in (**g**), except for X-linked gene expression, showing no dramatic differences across the clusters. **i**, Germline trajectory analysis for male FGCs[40], identified 7 clusters (0-6). Marker gene expression is given for these clusters. **j**, Box plots of the X/A ratios in male FCGs along the developmental trajectory defined in (**i**), showing an increase in cluster 2 relative to cluster 1. In total, n = 779 cells analyzed from published dataset[40] in **j**, Wilcoxon statistical testing used for (**c**-**f**) and (**j**). NS- Not Significant, * $p<0.05$, ** $p<0.01$, *** $p<0.001$.

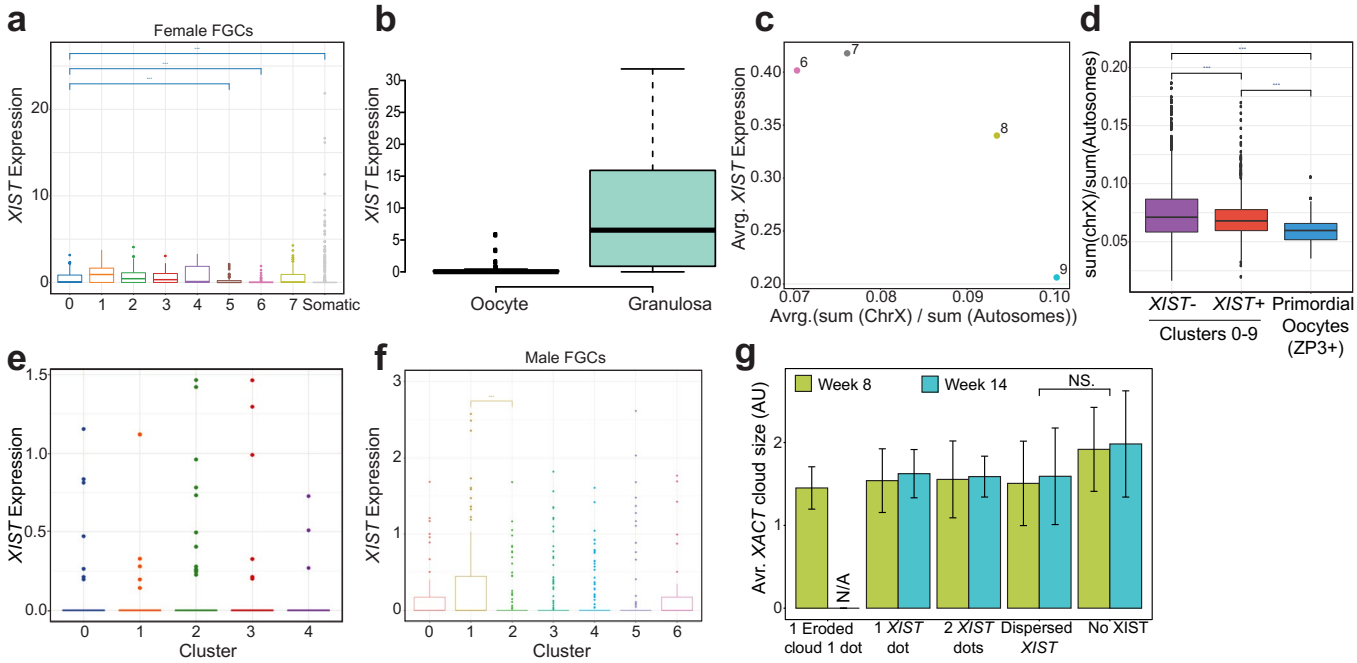

Extended Data Fig. 5 | *XIST* expression correlates with the X/A ratio. a, Boxplot depicting the expression of *XIST* in female germ cells organized by clusters along the developmental trajectory defined for the published FCG data set[40] in Extended Data Fig. 3f,g. *XIST* expression is significantly reduced from cluster 5 onwards. **b**, *XIST* expression in mature oocytes and granulosa cells from scRNA-seq data of adult ovary[44]. **c**, Scatter plot of average *XIST* expression (y-axis) and average X/A ratio (x-axis) for female germ cells clusters 6-9 (from Fig. 4d), capturing the entrance into meiosis. **d**, X/A ratios in female hPGCs and meiotic germ cells clustered based on expression of lncRNA *XIST*, *ZP3*+ primordial oocytes are clustered separately. **e**, Boxplots depicting *XIST* expression in male germ cells ordered along the developmental trajectory defined in Extended Data Fig. 4a–h, indicating that *XIST* transcripts are rarely detected in male germ cells. **f**, As in (e), except for male FGCs[40] from Extended Data Fig. 4i,j. **g**, Average *XACT* cloud size in week 8 and 14 pf hPGCs with different patterns of *XIST* expression, error bars show standard deviation of the cloud sizes (76 cells analyzed in total from 2 independent experiments). Wilcoxon statistical testing used for (**a**), (**d**), (**f**), (**g**). NS- Not Significant, * p<0.05, ** p<0.01, *** p<0.001. Number of cells analyzed across 5 independent experiments: **a. n =** 1016 cells[40], **b. n =** 148 cells[44], **d. n =** 1938 cells, **f**, n = 779 cells[40].

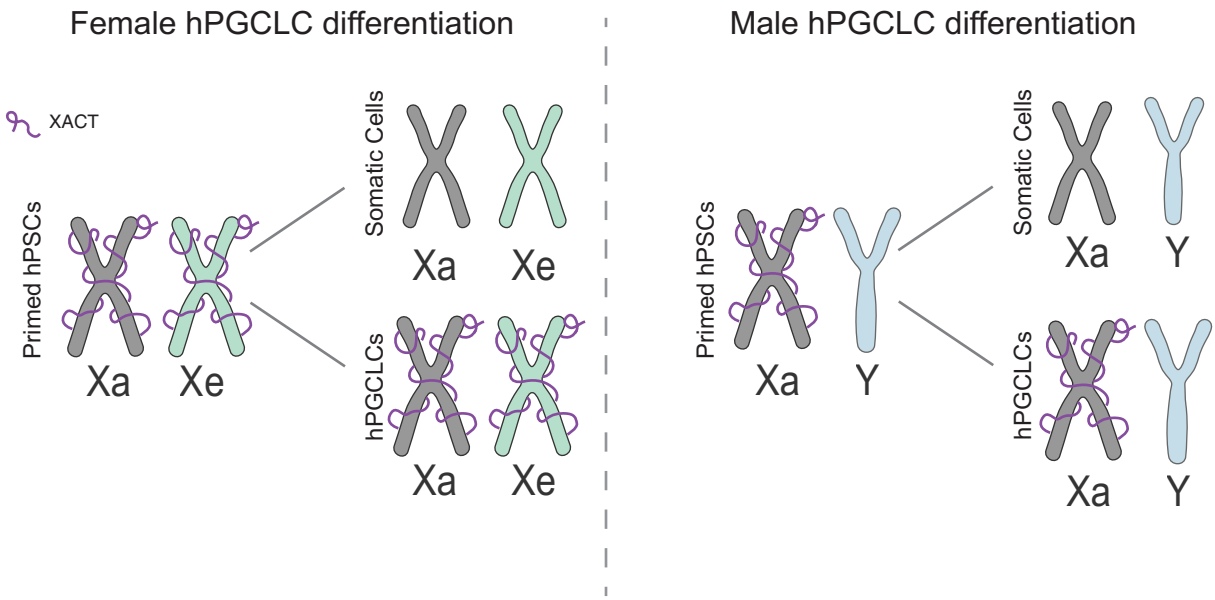

Extended Data Fig. 6 | *XACT* marks male and female hPGCLCs *in vitro*. Summary of the hPSC differentiation figure shown in Fig. 2. Due to XCI erosion, *XACT* is expressed from the Xa and the eroded X-chromosome in primed, female human pluripotent stem cells. The Xe state is transmitted into differentiated cells and upon hPGCLC differentiation. Moreover, *XACT* is maintained in hPGCLCs, whereas somatic cells silence *XACT*. Consequently, female hPSC-derived PGCLCs carry two *XACT* clouds and male hPSC-derived PGCLCs one.

nature research

Corresponding author(s): Kathrin Plath and Amander Clark

Last updated by author(s): Oct 17, 2020

Reporting Summary

Nature Research wishes to improve the reproducibility of the work that we publish. This form provides structure for consistency and transparency in reporting. For further information on Nature Research policies, see our Editorial Policies and the Editorial Policy Checklist.

Statistics

For all statistical analyses, confirm that the following items are present in the figure legend, table legend, main text, or Methods section.

n/a	Confirmed	
☐	☒	The exact sample size (*n*) for each experimental group/condition, given as a discrete number and unit of measurement
☐	☒	A statement on whether measurements were taken from distinct samples or whether the same sample was measured repeatedly
☐	☒	The statistical test(s) used AND whether they are one- or two-sided *Only common tests should be described solely by name; describe more complex techniques in the Methods section.*
☒	☐	A description of all covariates tested
☒	☐	A description of any assumptions or corrections, such as tests of normality and adjustment for multiple comparisons
☐	☒	A full description of the statistical parameters including central tendency (e.g. means) or other basic estimates (e.g. regression coefficient) AND variation (e.g. standard deviation) or associated estimates of uncertainty (e.g. confidence intervals)
☐	☒	For null hypothesis testing, the test statistic (e.g. *F*, *t*, *r*) with confidence intervals, effect sizes, degrees of freedom and *P* value noted *Give P values as exact values whenever suitable.*
☒	☐	For Bayesian analysis, information on the choice of priors and Markov chain Monte Carlo settings
☒	☐	For hierarchical and complex designs, identification of the appropriate level for tests and full reporting of outcomes
☒	☐	Estimates of effect sizes (e.g. Cohen's *d*, Pearson's *r*), indicating how they were calculated

Our web collection on statistics for biologists contains articles on many of the points above.

Software and code

Policy information about availability of computer code

Data collection	Custom scripts used for aligning population RNA-seq, scRNA-seq, data processing and plotting are available upon request
Data analysis	For scRNA-seq data analysis Scanpy v1.4.7, louvain 0.6.1. Cellranger v2.2. FACs sorting data was analyzed with FlowJo v10. R packages: ggsignif_0.6.0, data.table_1.12.0, ggplot2_3.3.0, reshape_0.8.8, biomaRt_2.38.0

For manuscripts utilizing custom algorithms or software that are central to the research but not yet described in published literature, software must be made available to editors and reviewers. We strongly encourage code deposition in a community repository (e.g. GitHub). See the Nature Research guidelines for submitting code & software for further information.

Data

Policy information about availability of data

All manuscripts must include a data availability statement. This statement should provide the following information, where applicable:

- Accession codes, unique identifiers, or web links for publicly available datasets
- A list of figures that have associated raw data
- A description of any restrictions on data availability

The accession number for the scRNA-seq data of prenatal tissues reported in this paper are GSE143380 (female cell data) and GSE143356 (male cell data). scRNA-seq data sets are also available for interactive exploration at http://germline.mcdb.ucla.edu.

Field-specific reporting

Please select the one below that is the best fit for your research. If you are not sure, read the appropriate sections before making your selection.

☒ Life sciences ☐ Behavioural & social sciences ☐ Ecological, evolutionary & environmental sciences

For a reference copy of the document with all sections, see nature.com/documents/nr-reporting-summary-flat.pdf

Life sciences study design

All studies must disclose on these points even when the disclosure is negative.

Sample size	Sample size was determined by availability of human prenatal tissues.
Data exclusions	No data was excluded, all biological samples received for this study were used either for scRNA-seq or immuno-RNA FISH experiments, no . Following scRNA-seq, genes expressed in less than five cells were discarded, and cells with less than 250 detected genes were filtered out.
Replication	All experiments on individual biological samples were performed in technical replicates. Human prenatal gonadal samples were each considered a single replicate and where possible results in scRNA-seq were verified by immuno-RNA FISH.
Randomization	This study did not involve comparison between experimental and control groups. For immuno-RNA FISH experiments random sections of the tissue were selected for staining
Blinding	This study did not use blinding for data analysis as the prenatal gonadal samples sent to us were already identified as male or female.

Reporting for specific materials, systems and methods

We require information from authors about some types of materials, experimental systems and methods used in many studies. Here, indicate whether each material, system or method listed is relevant to your study. If you are not sure if a list item applies to your research, read the appropriate section before selecting a response.

Materials & experimental systems

n/a	Involved in the study
☐	☒ Antibodies
☐	☒ Eukaryotic cell lines
☒	☐ Palaeontology and archaeology
☒	☐ Animals and other organisms
☐	☒ Human research participants
☒	☐ Clinical data
☒	☐ Dual use research of concern

Methods

n/a	Involved in the study
☒	☐ ChIP-seq
☐	☒ Flow cytometry
☒	☐ MRI-based neuroimaging

Antibodies

Antibodies used	Rabbit anti-human NANOG Abcam Cat#ab109250 1/200; Goat anti-human OCT4 Santa Cruz Cat#sc-8628 1/200; Rabbit anti-human H3K27me3 Millipore Cat#07-449 1/400; Mouse anti-human DAZL Santa Cruz Cat#sc-390929 1/400; BV421 conjugated anti-human/mouse CD49f (ITGA6) BioLegend Cat#313624 1/60; Alexa Fluor 488-conjugated anti-human CD326 (EPCAM) BioLegend Cat#324210 1/60.
Validation	NANOG antibody was validated the manufacturer, in human seminoma tissues by IHC and as Negative control PBS was used as a primary antibody. OCT4 antibody was published before in Chen et al. BOR 2017. H3K27me3 antibody was published before in Gell et al. Stem Cell Research 2018. DAZL antibody was published before in Kuo, P.L., et al. Fertil. Steril. 2004. ITGA6 and EPCAM antibodies were published in Chen et al. BOR 2017

Eukaryotic cell lines

Policy information about cell lines

Cell line source(s)	UCLA2 (46, XY) hESC lines were generated at UCLA from single blastocyst and published in Diaz et al., Human Molecular Genetics 2012. Female MZT04 hIPSC (46, XX) was generated by reprogramming human fibroblasts into iPSCs using Sendai virus Reprogramming (CytoTune) and published in Pandolfi et al., Stem Cell Research 2019.
Authentication	UCLA2 was authenticated by SNP/CNV analysis, MTZ04 was authenticated using Short tandem repeat analysis to the parental fibroblasts..

Mycoplasma contamination	All lines were routinely tested for mycoplasma contamination and tested negative
Commonly misidentified lines (See ICLAC register)	No commonly misidentified lines were used in this study

Human research participants

Policy information about studies involving human research participants

Population characteristics	The human subjects research portion of this project included pre-implantation embryo donors and fetal tissue. The pre-implantation embryo donors were couples who had sought treatment for infertility at an in vitro fertilization clinic. As a result of this treatment, the donors generated surplus embryos that were frozen. For the fetal tissues, donors were women of reproductive age who were seeking an elected termination of pregnancy.
Recruitment	Recruitment of embryo donors involved sending a UCLA IRB approved flyer to collaborating IVF laboratories. The laboratories provided the flyer to patients with frozen surplus embryos. The flyer contained details on the project, and UCLA contact details for additional information. Patients interested in donating embryos would then contact UCLA to be recruited into the study. No payments were made to clinics or donors for surplus embryos.
Ethics oversight	Use of human pre-implantation embryos in this research project followed California State law and the 2016 ISSCR guidelines for Stem Cell Research. Specifically, this involved annual review and approval by the UCLA Institutional Review Board (IRB) and the human embryonic stem cell research oversight committee (ESCRO) . Together, these committees approve the process of informed consent, and experiments using human embryos for research purposes . Patients were not paid for participation, and all donors were informed that the embryos would be destroyed as part of the research study. For fetal tissue samples provided by the University of Washington, regulatory oversight involved the University of Washington IRB approved Human Subjects protocol, combined with a Certificate of Confidentiality from the Federal Government. For fetal samples received from the University of Tübingen, the research project was also approved by the research ethics committee of the University of Tübingen. No payment was made to fetal tissue donors, and all patient identifiers were removed before shipping to UCLA.

Note that full information on the approval of the study protocol must also be provided in the manuscript.

Flow Cytometry

Plots

Confirm that:

☒ The axis labels state the marker and fluorochrome used (e.g. CD4-FITC).

☒ The axis scales are clearly visible. Include numbers along axes only for bottom left plot of group (a 'group' is an analysis of identical markers).

☒ All plots are contour plots with outliers or pseudocolor plots.

☒ A numerical value for number of cells or percentage (with statistics) is provided.

Methodology

Sample preparation	hPGCLC aggregates were dissociated 0.05% Trypsin-EDTA (GIBCO, 25300-054) for 10 min at 37o C. The dissociated cells were stained with conjugated antibodies, washed with FACS buffer (1% BSA in PBS) and resuspended in FACS buffer with 7-AAD (BD PharMingen, 559925) as viability dye. The conjugated antibodies used in this study include ITGA6 conjugated with BV421 (BioLegend, 313624, 1:60), EPCAM conjugated with 488 (BioLegend, 324210, 1:60). The single cell suspension was sorted for further experiments using BD FACSAria fluorescence-activated cell sorting machine. FACS data was analyzed with FlowJo v10 software. Double positive cells for ITGA6 and EPCAM (hPGCLCs) and negative cells (non-hPGCLCs) were collected in hPGCLC media and plated on human plasma fibronectin coated coverslips overnight. Following morning, RNA FISH was performed using the coverslips.
Instrument	BD FACSAria
Software	Manufacturers software was used for sorting. Data analysis was done using FlowJo v10
Cell population abundance	Double positive hPGCLC population was sorted using EPCAM and ITGA6. Abundance of cell population indicated in the figure. All somatic cells were selected outside hPGCLC gate
Gating strategy	Gating was done by single color staining of hESCs. Complete strategy is provided in the supplementary information

☒ Tick this box to confirm that a figure exemplifying the gating strategy is provided in the Supplementary Information.